2022-06

IMPROVING THE FLEXIBILITY AND THERMAL PROTECTION OF A DIVING WETSUIT

Waldron, Andrew T.

Monterey, CA; Naval Postgraduate School

NAVAL POSTGRADUATE SCHOOL

MONTEREY, CALIFORNIA

THESIS

IMPROVING THE FLEXIBILITY AND THERMAL PROTECTION OF A DIVING WETSUIT

by

Andrew T. Waldron

June 2022

Thesis Advisor: Emil P. Kartalov
Co-Advisor: Claudia C. Luhrs

THIS PAGE INTENTIONALLY LEFT BLANK

REPORT DOCUMENTATION PAGE			Form Approved OMB No. 0704-0188

1. AGENCY USE ONLY *(Leave blank)*	2. REPORT DATE June 2022	3. REPORT TYPE AND DATES COVERED Master's thesis

4. TITLE AND SUBTITLE IMPROVING THE FLEXIBILITY AND THERMAL PROTECTION OF A DIVING WETSUIT	5. FUNDING NUMBERS RPQC5
6. AUTHOR(S) Andrew T. Waldron	
7. PERFORMING ORGANIZATION NAME(S) AND ADDRESS(ES) Naval Postgraduate School Monterey, CA 93943-5000	8. PERFORMING ORGANIZATION REPORT NUMBER
9. SPONSORING / MONITORING AGENCY NAME(S) AND ADDRESS(ES) Office of Naval Research	10. SPONSORING / MONITORING AGENCY REPORT NUMBER

11. SUPPLEMENTARY NOTES The views expressed in this thesis are those of the author and do not reflect the official policy or position of the Department of Defense or the U.S. Government.

12a. DISTRIBUTION / AVAILABILITY STATEMENT Approved for public release. Distribution is unlimited.	12b. DISTRIBUTION CODE A

13. ABSTRACT (maximum 200 words)

This research improves the thermal protection and mobility of divers by incorporating a silicone glass microsphere composite, cast in geometries that adapt to various body curvatures, into a conventional neoprene wetsuit. These geometries are designed such that an array of trapezoidal teeth—on a thin base of the same material—converge together to approximate curved body shapes. Previous composite wetsuit designs, including a similar glass microsphere composite, derive each composite piece from 3D body scans. This design generalizes one geometry to apply to a range of body curves. This method reduces variance in mold designs, reduces mold sizes, and reduces cost and maintenance for composite wetsuit molds. With this approach, composite wetsuit materials can be more rapidly prototyped and eventually incorporated into wetsuits that protect professional Navy divers. The thermal protection of this material was validated experimentally at set curvatures in varying pressure environments. Additionally, the material was added to a 3-millimeter wetsuit and tested in a real salt-water environment. The composite's porosity was reduced and compared using optical microscopy. Thermal metrics from experimental and diving results were compared to previous prototypes.

14. SUBJECT TERMS diving, thermal protection, manufacturing methods, microspheres, composite, silicone, casting, 3D printing	15. NUMBER OF PAGES 117
	16. PRICE CODE

17. SECURITY CLASSIFICATION OF REPORT	18. SECURITY CLASSIFICATION OF THIS PAGE	19. SECURITY CLASSIFICATION OF ABSTRACT	20. LIMITATION OF ABSTRACT
Unclassified	Unclassified	Unclassified	UU

NSN 7540-01-280-5500

Standard Form 298 (Rev. 2-89)
Prescribed by ANSI Std. 239-18

THIS PAGE INTENTIONALLY LEFT BLANK

Approved for public release. Distribution is unlimited.

IMPROVING THE FLEXIBILITY AND THERMAL PROTECTION OF A DIVING WETSUIT

Andrew T. Waldron
Ensign, United States Navy
BS, United States Naval Academy, 2021

Submitted in partial fulfillment of the
requirements for the degree of

MASTER OF SCIENCE IN MECHANICAL ENGINEERING

from the

NAVAL POSTGRADUATE SCHOOL
June 2022

Approved by: Emil P. Kartalov
Advisor

Claudia C. Luhrs
Co-Advisor

Garth V. Hobson
Chair, Department of Mechanical and Aerospace Engineering

THIS PAGE INTENTIONALLY LEFT BLANK

ABSTRACT

This research improves the thermal protection and mobility of divers by incorporating a silicone glass microsphere composite, cast in geometries that adapt to various body curvatures, into a conventional neoprene wetsuit. These geometries are designed such that an array of trapezoidal teeth—on a thin base of the same material—converge together to approximate curved body shapes. Previous composite wetsuit designs, including a similar glass microsphere composite, derive each composite piece from 3D body scans. This design generalizes one geometry to apply to a range of body curves. This method reduces variance in mold designs, reduces mold sizes, and reduces cost and maintenance for composite wetsuit molds. With this approach, composite wetsuit materials can be more rapidly prototyped and eventually incorporated into wetsuits that protect professional Navy divers. The thermal protection of this material was validated experimentally at set curvatures in varying pressure environments. Additionally, the material was added to a 3-millimeter wetsuit and tested in a real salt-water environment. The composite's porosity was reduced and compared using optical microscopy. Thermal metrics from experimental and diving results were compared to previous prototypes.

THIS PAGE INTENTIONALLY LEFT BLANK

Table of Contents

List of Figures

THIS PAGE INTENTIONALLY LEFT BLANK

List of Tables

THIS PAGE INTENTIONALLY LEFT BLANK

List of Acronyms and Abbreviations

°C	degrees Celsius
°F	degrees Fahrenheit
1D	One dimensional
3D	Three dimensional
α	Arc Curvature Angle
β	Tooth Angle
δ	deformation
Δ**T**	Temperature Difference
ϵ	emissivity
θ	Tooth Draft Angle
Θ	Insulance
ν	Poisson's Ratio
ρ	Effective Resistivity
σ_b	Stefan-Boltzmann constant
ϕ	Heat Flux
ϕ_c	convection
ϕ_d	conduction
ϕ_e	evaporation
ϕ_r	radiation

a	Arc Length
A	Surface Area
BC	Buoyancy Compensator
c	Chord Length
C	Circumference
c_p	heat capacity
D	Diameter
EDO	Engineering Duty Officer
EOD	Explosive Ordnance Disposal
E	Elastic Modulus
F	force
fsw	feet of seawater
h	Convective Heat Coefficient
HGM	Hollow Glass Microspheres
h_t	Tooth Height
H	Total Composite Thickness
i	Current
k	Thermal Conductivity
kPa	kilopascals
mL	milliliter
mm	millimeter
msw	meters of seawater

N Tooth Number

ND Navy Divers

NEDU Navy Experimental Diving Unit

NPS Naval Postgraduate School

ONR Office of Naval Research

psi Pounds Per Square Inch

PC Polycarbonate

PDMS Polydimethylsiloxane

P_e Electrical Power

r Radius of Curvature

R Thermal Resistance

R_{θ_s} Equivalent Series Resistance

R_{θ_p} Equivalent Parallel Resistance

rpm Rotations Per Minute

s Body Curve Length

S Outer Curve Length

SEM Scanning Electron Microscope

SSDS surface support diving system

SEAL Sea, Air, and Land

SCUBA Self-Contained Underwater Breathing Apparatus

t Base Thickness

USH Underwater Ship's Husbandry

UDT Underwater Demolition Team

USN U.S. Navy

V Voltage

w_t Top Tooth Width

W_t Bottom Tooth Width

W Watts

WWII World War II

Acknowledgments

I would like to acknowledge my advisors Dr. Emil Kartalov and Dr. Claudia Luhrs for guiding me through the development of this thesis. I'd also like to thank the Office of Naval Research (ONR) for funding this project. Diving operations open the scope of our Navy. ONR's continued support allows us to develop diving technology that enhances the endurance and lethality of our Naval forces.

I'd also like to thank Ruth "Cricket" Justice-Limes of Otter Bay Wetsuits in Monterey, CA for helping fabricate this wetsuit prototype. Her work has enabled Naval Postgraduate School (NPS) students to test their wetsuit designs in real seawater environments. Experiments would also not have been possible without the guidance and feedback of local dive shops in Monterey. Special thanks are due to Bamboo Reef, Aquarius, and Cannery Row Aquatics dive shops.

I would also like to acknowledge the assistance of my diving partners, 2d Lt Nicohl Corretjer, ENS Alexander Tum, and Kostas Meligkaris. Diving with a buddy was critical to safe experiments to test the suit's real performance in seawater.

Special thanks to Dr. Chanman Park for conducting some compression tests that measured the mechanical properties of the composite material to failure.

Finally, I'd like to thank all family, friends, and colleagues who supported me and my research at NPS.

THIS PAGE INTENTIONALLY LEFT BLANK

CHAPTER 1:
Introduction

1.1 History of Naval Diving

Although diving has consistent tactical advantages, diving technology has drastically changed throughout history and has extended missions to greater working limits. Military diving has enabled the U.S. Navy (USN) to salvage valuable material, clear obstructions, and subvert its enemies. During the Civil War, divers cleared Mobile Bay of Confederate mines. After Pearl Harbor Navy Divers (ND) returned four of the six targeted battleships to the Pacific. Salvaged enemy ships also provided key intelligence such as code books and secret war plans. In the European theater, Underwater Demolition Team (UDT) Teams destroyed obstacles on Normandy beach, which led to a successful allied invasion. Today's Navy Sea, Air, and Land (SEAL) Teams, shown in Figure 1.1, are direct descendants of these UDT teams [1].

Figure 1.1. A Navy SEAL Team emerges from the water during an insertion exercise. Diving operations enable the rapid insertion and extraction of special forces in global hot spots. Source: [2].

In contrast to combat diving Underwater Ship's Husbandry (USH) in Figure 1.2, deep submergence diving, and saturation diving all sustain naval ship readiness. USH in particular allows the Navy to do maintenance on ships without the expensive process of bringing them into drydock [3]. Enlisted ND are primarily responsible for this underwater maintenance. Engineering Duty Officer (EDO) Divers within the Surface Warfare and Submarine communities as well as SEABEEs also contribute to USH and underwater construction.

Figure 1.2. NDs are the U.S. Navy's main diving authority. Sources: [4].

While responsible for diving maintenance, these divers also support special forces, ships, and submarines as diving subject matter experts. NDs also research the physiological limits of diving at the Navy Experimental Diving Unit (NEDU) in Panama City, FL [3]. Divers aboard fast-attack submarines also conduct ship routine security inspections of the hull when entering and exiting port. These divers also do simple maintenance, such as removing obstructions from the ship's propeller or valves.

1.2 Introduction of the Diving Wetsuit

The introduction of Self-Contained Underwater Breathing Apparatus (SCUBA) and decompression tables in the late 1920s led to longer dives in colder waters [1]. The invention of

the wetsuit was intended to improve the thermal protection for frogmen. Previously, combat divers donned long johns or coated themselves in grease for thermal protection, as seen in Figure 1.3.

Figure 1.3. Frogmen in World War II (WWII) lacked proper thermal protection when swimming [5]. Source: [6].

UDTs often covered themselves in grease prior to diving missions [5] and wore swim trunks. They only wore a few accessories: goggles, fins, and a combat knife [7]. Without proper protection and in water 21.11 degrees Celsius (°C) (70 degrees Fahrenheit (°F)) or less, a diver loses more heat faster than the body can regenerate it [8]. A diver cannot think or work as clearly when cold. In these conditions, the risk of hypothermia and decompression sickness increases, both of which can lead to death [8]. A wetsuit provides passive warmth to a diver, trapping a thin layer of water between the diver's skin and the suit. It improves comfort and is easier to equip than other diving dress [8].

From 1918-1984 salvage divers wore the Mark V Diving dress in Figure 1.4, made of a rubber canvas, that sealed out all water. The innovation of rubber cuffs and neck lining in this suit also enabled divers to swim in contaminated waters.

Figure 1.4. Mark V Diving Dress [9].

Similar to the Mark V diving dress, the modern dry suit is fully sealed. Unlike a wetsuit, a dry suit, as the name suggests, keeps a diver completely dry. The clothing worn underneath the suit alone warms the diver. The main limitation of this feature is that, if the suit rips, the diver is fully compromised to the cold environment and must abandon a job.Many divers often wear wetsuits underneath their dry suit for added thermal protection [9]. Many deep submergence diving suits also feed in warm water into the diving dress to actively heat the diver [1].

Cold water divers often choose to wear a thicker neoprene wetsuits between five and eight millimeters [10] as seen by the surface supply diver in Figure 1.5. These divers work on vessels with drafts ranging from about 27 to 52 feet of sea water [11]. Combat divers also stay at relatively shallow depths, travelling long distances underwater and hovering to and from insertion or extraction points.

Figure 1.5. A Surface Supply Diver lunges into the water wearing a thick wetsuit to begin a dive. Source: [1].

Wetsuits are a popular choice among divers because they are easy to use and equip, while dry suits require additional training to control buoyancy and maintenance. Since 1985, the Navy's official diving dress has been the Mark 12 surface support diving system (SSDS), a combination of a neoprene wetsuit and a more durable jumpsuit, that protects the diver from abrasion. Most of a diver's internal heat exits from the head and extremities. To mitigate this heat loss, divers wear diving hoods, gloves, and boots. Depending on conditions this equipment is vital to a diver's performance and health [1]. However, the material properties of today's modern day wetsuits may alone be insufficient in keeping divers safe at depth for extended periods of time.

1.3 Wetsuit Properties

The inventor of the wetsuit, Hugh Bradner, challenged the belief that to stay warm you had to stay dry. Bradner invented the wetsuit to provide Navy frogmen with better thermal protection [5]. Bradner field tested his suit while SCUBA diving, seen in Figure 1.6.

Figure 1.6. Hugh Bradner, the inventor of the wetsuit, enters the water with his diving buddy, Charlie Townes, on Ano Nuevo Island in 1953. Source: [9].

Most wetsuits are made of neoprene, a closed cell rubber foam that contains either air or nitrogen pores [12]. In a closed cell neoprene suit, a thin layer of water between the suit and the diver's skin warms the diver [8]. Thicker suits have increased Insulance (Θ) but are less maneuverable. This restricted motion fatigues the diver at the expense of more air. Added thickness increases buoyancy, and a diver must attach more weight to compensate [8]. As a diver descends in the water column, the wetsuit compresses with increasing hydrostatic pressure [8]. The pores within the neoprene collapse, and the material becomes thinner [12]. Compounded together these effects reduce the neoprene's Θ, equal to the fraction of Temperature Difference (ΔT) and Heat Flux (ϕ), given in Equation 1.1 [13].

$$\Theta = \frac{\Delta T}{\phi} \tag{1.1}$$

This extensive property is the basis for determining and comparing the thermal protection of different wetsuit materials experimentally and in real diving scenarios.

CHAPTER 2:
Literature Review

2.1 Heat Transfer of the Human Body in Water

An immersed human body loses more heat at a higher rate in water than in air of the same temperature. This fact is the result of water's adverse thermal properties. Water has a 1000 times greater heat capacity (c_p) and a 25 times greater Thermal Conductivity (k) than air's. Rapid heat loss in divers poses a serious health risk that could result in injury or death. The Navy's Medical Research Institute defines hypothermia as: "A condition in which the deep tissue or 'core' temperature of the body is below the normal physiological range, about 37 °C (98.6 °F) [14]." Exposure to water for extended periods of time has a significant impact on mental cognition and physical dexterity. USN divers routinely train in extreme temperature conditions, described in Figure 2.1.

Figure 2.1. Divers from the Mobile Dive Salvage Unit and Underwater Construction Unit in Pearl Harbor, HI dive beneath Arctic ice for the Navy's 2022 ICEX. These divers practiced finding and recovering submarine torpedoes in the coldest and most confined conditions possible. Source: [15].

The body's total heat loss is collectively the sum of its individual heat losses by conduction (ϕ_d), convection (ϕ_c), radiation (ϕ_r), and evaporation (ϕ_e) in Equation 2.1 [14].

$$\phi_n = \phi_c + \phi_d + \phi_r + \phi_e \tag{2.1}$$

Heat losses vary among divers based on many factors that can be difficult to fully quantify including experience, breath rate, metabolism, and body composition. To model heat transfer in a diver requires clear definition of assumptions.

Evaporative heat losses can be neglected, as perspiration in cold water does not occur [14]. Convective heat losses during respiration and movement in water have more detailed assumptions. During respiration a person transfers heat to the air. For divers breathing on SCUBA, the temperature of the air they breathe depends on the temperature of the air in their tanks, which changes with depth. Divers can also have different breath rates due to a variety of factors, such as experience, activity, and metabolism. A less experienced diver may consume more air due to anxiety or stress. More demanding activities, like underwater construction, put a greater physical load on divers. High stress activity can cause the body to generate more heat, as a diver is working harder. A person's metabolic needs for aerobic and anaerobic activity affect a divers air consumption as well [10].

In [10] a model for immersed divers specifies the body's power generation in a range of 80 to 140 Watts (W). Movement in water adds further complexities. While swimming a diver generates more or less heat depending on swim speed. Movement through the water forces water to flow across the body in forced convection [16]. Given low speed and untracked speed throughout dives in this research, convective heat losses can be assumed to be natural convection, given in Equation 2.2, where Convective Heat Coefficient (h) is a constant, A_{diver} is the surface area of the diver's body, and T_{out} is the external surface temperature of the suit.

$$q = hA_{diver}(T_{out} - T_{\infty_w}) \tag{2.2}$$

Conduction is the predominant heat transfer mechanism for an immersed body in water, driven by the difference between water temperature and the body's core temperature [14], given in Equation 2.3.

$$q = \frac{k(T_i - T_\infty)A}{\Delta x} \tag{2.3}$$

Biological differences among divers have an even greater effect on conduction to the surrounding water. Besides the additional thermal protection divers elect to wear, their tissue and fat thickness can reduce their heat loss by a factor of 15 [14]. Overall, the biological differences of divers impact their heat transfer to their environment.

Specifically for wetsuits, the thickness of the water layer between a wetsuit and the diver's skin affects heat loss by conduction. If water layer in the wetsuit is too thick, the diver cannot produce enough heat to passively warm it. Essentially, the passive warming mechanism of the suit can fail if the internal water layer is too thick.

When discussing heat transfer of a body in air, radiation heat losses are considered [10]. The radiation of heat to the surrounding water is also accounted with the first order Taylor expansion of the Stefan-Boltzmann law in Equation 2.4, with variables emissivity (ϵ) and Stefan-Boltzmann constant (σ_b) are constants and T_{out} equal to the suit's external surface temperature in Kelvin .

$$q = 4A\epsilon\sigma_b T_{out}^3 (T_{out} - T_i) \tag{2.4}$$

2.1.1 Modeling Heat Transfer of an Immersed Diver

When combining all of these heat transfer mechanisms into one model, an analogy between electrical flow in circuits and heat flow can be made [17]. This comparison is derived from Ohms law (Equation 2.5), where the electrical potential across a resistor is equal to the current,

$$i = \frac{V}{R} \tag{2.5}$$

or the ΔT across Thermal Resistance (R) is equal to heat flow in Equation 2.6.

$$q = \frac{\Delta T}{R} \tag{2.6}$$

Like electrical resistors, thermal resistors in series have the same heat flow like current, but they have different ΔTs or electrical potentials. In parallel, resistors have the same ΔT, but heat is split among the resistors. A schematic showing the difference between the two types of thermal resistance networks is given in Figure 2.2.

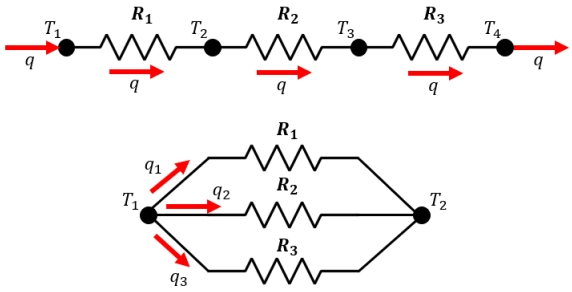

Figure 2.2. A Series Thermal Resistance Network (top) is a linear arrangement of thermal resistors, while a Parallel Thermal Resistance Network (bottom) connects multiple thermal resistors with identical temperature nodes. Source: [17].

Equivalent Series Resistance (R_{θ_s}) can simply be added together in Equation 2.7,

$$R_{\theta_s} = \sum R_i \tag{2.7}$$

while Equivalent Parallel Resistance (R_{θ_p}) must be converted to an equivalent series resistor in Equation 2.8 to be summed.

$$R_{\theta_p} = \left(\sum \frac{1}{R_i} \right)^{-1} \tag{2.8}$$

2.1.2 Thermal Circuit of NPS Diving Experiments

The thermal resistance network, governing the heat transfer mechanism in [18] and [19], assumes:

- an unsteady heat transfer process where the temperature difference between the inside and outside of the suit changes with time.
- approximate ΔT between the suit inner wall and ambient seawater
- the inner suit temperature is an approximation of the warmest skin temperature
- the ambient water temperature can be measured by a similar temperature gauge attached to diving gear outside of the wetsuit.

- negligible conduction through tissue and fat
- negligible heat losses due to respiration

Although temperature measurements from the rectum, esophagus, or ear are more accurate approximations of core body temperature than skin temperature measurements as cited in [14], these more invasive thermometers were not used to approximate core body temperatures in Naval Postgraduate School (NPS) experiments. Skin thermometers that also tracked pressure with time were chosen as a more practical choice for continuously measuring ΔT with time throughout SCUBA dives.

With the given assumptions and defined heat transfer mechanisms, the thermal circuit for previous NPS diving experiments is drawn in Figure 2.3.

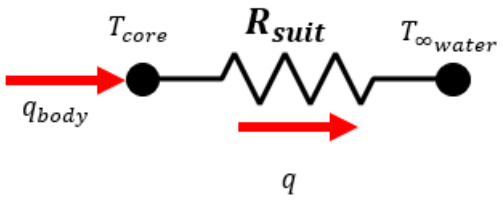

Figure 2.3. The drawn thermal circuit illustrates the heat transfer model of previous NPS SCUBA Diving Experiments

2.1.3 Alternative Thermal Models for Divers

Alternatively, a heat transfer model in [10] has different assumptions governing its heat transfer model:

- an unsteady heat transfer process in which the diver's body temperature drops to an unsafe level when exposed to water for long periods of time.
- a constant ambient water temperature
- significant losses by convection and radiation to the water
- conduction through tissue and fat, accounting for the diver's mass and heat capacity

- an approximate Θ through body tissue and fat from other literature
- a constant source of heat from the body

With the given assumptions and defined heat transfer mechanisms, the thermal circuit for this alternative model is drawn in Figure 2.4.

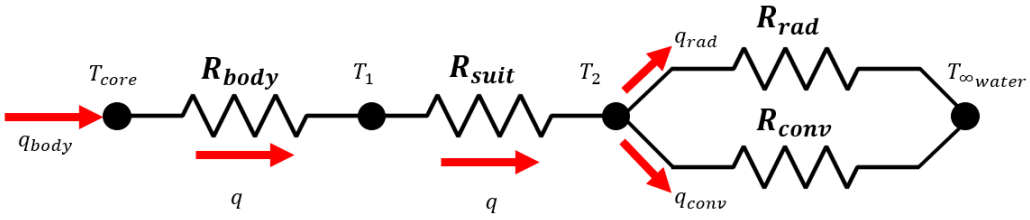

Figure 2.4. Immersed Diver Thermal Circuit with Radiation and Convection
Source: [10]

The drawn thermal circuit illustrates the heat transfer model of an unsteady heat transfer which includes thermal resistance for body tissue and a parallel resistor with radiation and convection terms. The equivalent resistance of this circuit is:

$$R_\theta = R_{body} + R_{suit} + \frac{R_{conv}R_{rad}}{R_{conv} + R_{rad}} \tag{2.9}$$

where in $[K/W]$,

$$\begin{aligned} R_{body} &\approx 0.03 \\ R_{suit} &= \frac{\Delta x}{kA} \\ R_{conv} &= \frac{1}{hA} \\ R_{rad} &= \frac{1}{4A\epsilon\sigma T_{out}^3} \end{aligned} \tag{2.10}$$

Ultimately, this model is used to predict the time at which a diver's temperature state

becomes unsafe to continue diving, which is generally defined in Equation 2.11.

$$t(T_i) = C_e M R_\theta \ln\left(\frac{qR_\theta + T_{\infty_w} - T_{io}}{qR_\theta + T_{\infty_w} - T_i}\right) \tag{2.11}$$

This unsafe time occurs at 27 °C, in which the body undergoes: "minor disorders that can turn into loss of consciousness, collapse, and even death [10]." Other literature from the infamous Dachau experiments suggests these physiological condition start a higher temperature of 30 °C [14]. As shown in Figure 2.5, the effect of wearing a thicker wetsuit extends a diver's survivable period underwater.

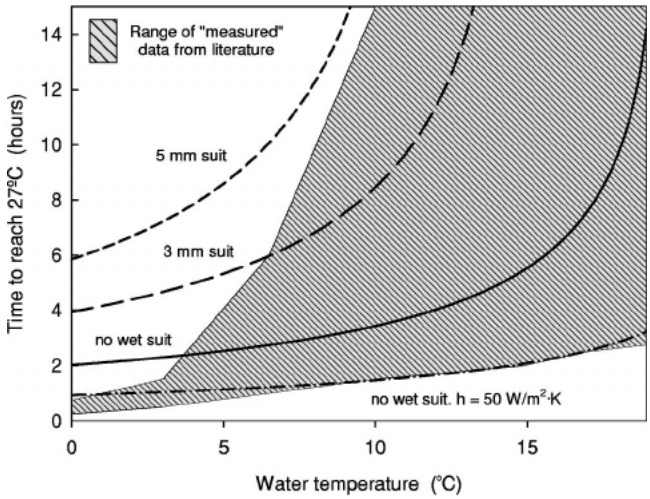

Figure 2.5. Time for Unsafe Diving Conditions for Various Diving Dress
Source: [10]

The effects of increasing the thermal resistance of the diver dress were modeled. Increasing wetsuit thickness improved the longevity of divers in cold water. Divers with no added thermal protection were estimated to live at minimum one hour. In conditions similar to the Pacific Ocean in Monterey, CA, where the diving research of these experiments are conducted, the water temperature is historically on average 13.33 °C (56 °F) year-round [20]. The coldest water temperatures typically occur in March at a low of 8.89 °C (48 °F), shown in Figure 2.6.

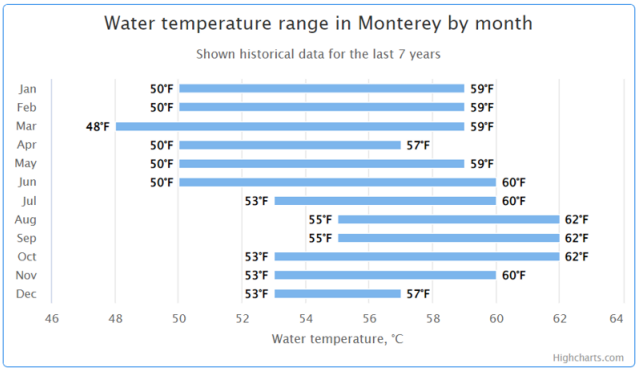

Figure 2.6. Historical Water Temperatures in Monterey, CA Source: [20]

This chart shows averages of a seven year water temperature history in Monterey, CA. The coldest month for SCUBA diving occurs in March. The survival times for a nude swimmer in minimum and average Monterey water temperatures are about one hour to an hour and a half. For a swimmer in a three millimeter (mm) wetsuit, that survival time extends to about five and a half to ten hours. Generally, as the neoprene's thickness and Θ increase, the minimum survival time plotted increases at 0 °C, and the function of survival time steepens, prolonging the onset of hypothermia.

2.1.4 Coordinate System Considerations

Coordinate system are important for defining boundary conditions of heat flow. The predominant mechanism studied in this research is conduction. One dimensional (1D) steady conduction with heat generation through Cartesian and a cylindrical bodies are governed by the following heat equations, as shown in Equation 2.12 and Equation 2.13 [17].

$$k\frac{d^2T}{dx^2} + \dot{q} = 0 \tag{2.12}$$

$$\frac{1}{r}\frac{d}{dr}\left(kr\frac{dT}{dr}\right) + \dot{q} = 0 \tag{2.13}$$

For complex geometries, a Cartesian system can be used [17]; however, when analyzing heat transfer through curved material, a cylindrical boundary condition may be more appropriate.

2.2 Properties NPS Composite Wetsuit Material

Understanding the heat transfer mechanisms of an immersed diver, improving the suit's thermal resistance is a realistic strategy for mitigating diver heat loss. The focus of this research and other NPS diving research is to experimentally quantify the Θ of wetsuit materials and to field test fully fabricated wetsuits in seawater environments [18] [19].

2.2.1 Thermal Properties of NPS Composite Material

Unlike neoprene's aerogel pores that collapse with depth, a stiffer silicone material embedded with Hollow Glass Microspheres (HGM) resists changes in Θ due to compression. This composite has been added to the features of a thinner neoprene wetsuit to enhance thermal protection without sacrificing flexibility. The HGMs physically maintain their shape and the volume of air inside them.

Experiments were conducted to compare Effective Resistivity (ρ) between composites with different loadings of HGM and to compare the Θ between the ideal HGM composite and neoprene with depth [21]. A schematic of this experimental setup is shown in Figure 2.7.

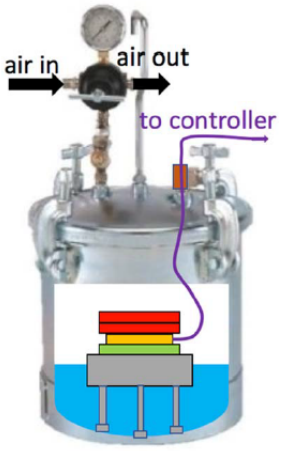

Figure 2.7. A cylindrical puck of the composite material (green) is placed between an adjustable aluminum stage (gray) in ice water and a temperature controlled heater (yellow). Additional composite pucks (red) were placed on top of the heater for insulation. This setup was modified to measure the Θ of flexible composite pieces in curved orientations. Source: [21]

The pressure was adjusted to correspond to various working depths, relevant to SCUBA operations. Θ was calculated from Equation 2.14 by dividing the known ΔT by ϕ,

$$\Theta = \frac{\Delta T}{\phi} \tag{2.14}$$

The ϕ through the material samples was equal to the Electrical Power (P_e) input from the heater, divided by the cross-sectional area of the heater. where P_e equaled was calculated from the product of the controller's measured Current (i) and Voltage (V)

$$P_e = iV \tag{2.15}$$

and where Surface Area (A) was for a puck was calculated from the its measured Diameter (D) in Equation 2.16

$$A = \frac{\pi D^2}{4} \tag{2.16}$$

Conceptually, the more P_e required to maintain the ΔT between the water and the heat, the less insulative the material is. The resulting equation for Θ in Equation 2.17 then becomes

$$\Theta = \frac{\Delta T}{\phi} = \frac{\pi D_h^2 (T_h - T_w)}{4 P_e} \tag{2.17}$$

The assumptions for this experiment were:

- 1D Steady State Heat Flow
- Negligible Convective and Radiation Heat Losses
- An Insulated Heater
- The Composite had Uniform Thermal Properties
- Cartesian Coordinate System

A graph comparing the Θ of eight mm neoprene and a 43% volume HGM composite is given in Figure 2.8.

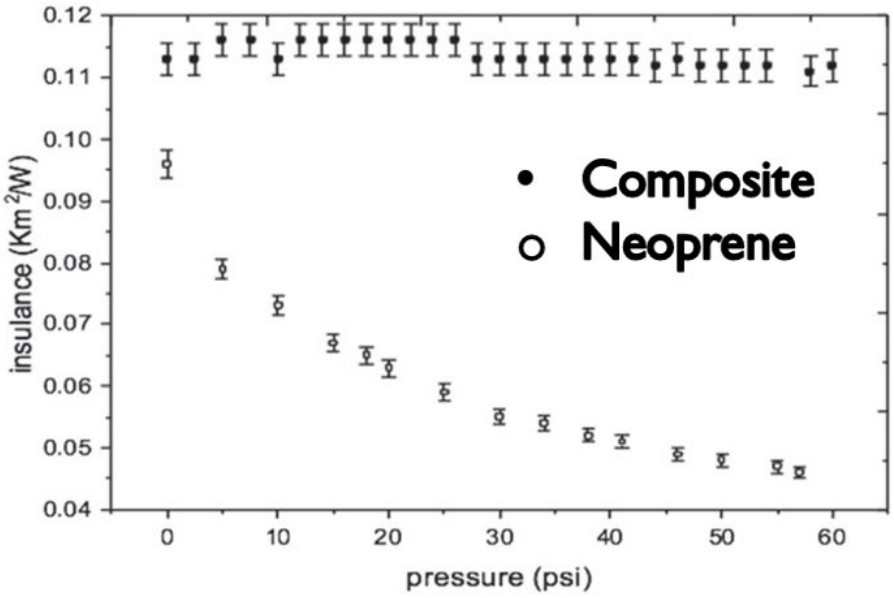

Figure 2.8. Depth Independent Composite Thermal Properties Source: [21]

In a variable pressure testing apparatus, the Θ of an eight mm Neoprene sample and the Composite with 43 percent volume of HGM were measured and compared. Neoprene's Θ decreased with pressure (simulating increasing water depth) while the composite's Θ maintained relatively constant thermal properties with depth.

While the Θ of the HGM composite was measured in a flat orientation, the composite was cast in curved dimensions. For incorporation into the wetsuit, composite pieces were cast in curved orientations, but their previous thermal properties were measured in a Cartesian coordinate system.

However, if applied to the entire suit, the rigidity of a composite restricts the diver's maneuverability. Attempts to create a suit entirely out of a composite foam have also been problematic because these prototypes were not as form fitting as neoprene suits. Improper tailoring led to cold water pockets filling the suit, which weaken its thermal protection [22].

2.2.2 Mechanical Properties of Syntactic Foams

A HGM silicone composite falls into a family of polymer syntactic foams. Often syntactic foams used in applications where large compressive stresses are a factor. A study of the compression response of syntactic foams to compression is necessary to produce the appropriate mechanical properties [23]. While this research project hinges on the use of syntactic foams to reduce the compression and insulance reduction of wetsuit composites, a study at NPS of the mechanical properties used diving wetsuits has not been conducted.

To understand a polymeric material's mechanical behavior, uniaxial compressive tests are often done to determine the material's stress strain curve [24]. Another method is simulating the response to compression is through a computational model [23]. The typical stress strain curve for a polymer under compressive loading is given in Figure 2.9.

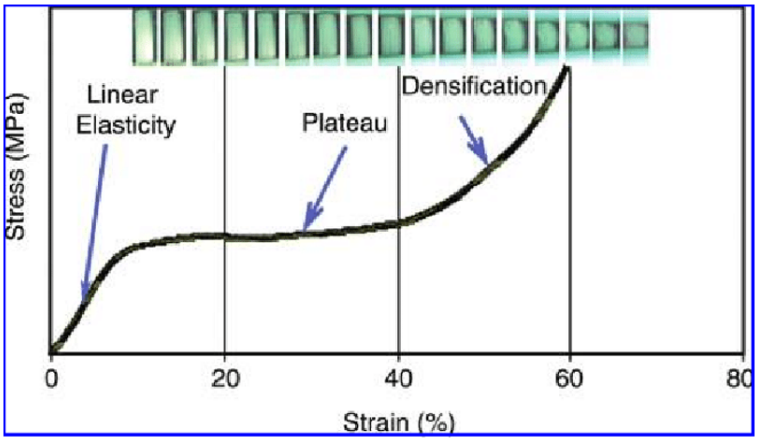

Figure 2.9. A stress strain curve for a polymer under compression is divided into three zones: linear, elastic, plateau, and densification. Source: [24]

Initially, when loaded a polymer material experiences linear elastic stress, where stress increases at a constant rate. Then, the material's stress plateaus to a constant stress. Finally, the stress rapidly increases as its density reaches a certain threshold [24]. Higher volumetric percentages of HGM increase the yield strength of the composite and densification stress, while the energy absorbed decreases. However, the yield strength changes with the wall thickness of the sample a syntactic foam sample. Thicker foams take more stress to yield, as their internal HGMs have higher compressive strength than thinner foams [23].

2.3 Approaches to Improving the Thermal Protection of Wetsuits

The combination of both neoprene and stiff composites is necessary to improve the suit's thermal performance with depth without sacrificing flexibility. Several students at the NPS individually cast HGM composites to their bodies and added it to custom neoprene wetsuits. This technique was analogous to armor plating [19]. These wetsuit prototypes were eventually tested in a real seawater environment and compared to conventional cold water diving wetsuits of seven mm in uniform thickness. The process to design, fabricate, and incorporate these pieces onto a thinner three mm wetsuit is included in Figure 2.10.

Figure 2.10. (A) A full body scan rendered the geometry to be approximated for individual casting (B) Areas of the scan were cut into individual pieces to be cast (C/D) The curved positive geometry was then converted into a mold (E) The HGM composite was cast in each body curve shape (F/G) All finished pieces were laid out on a thin custom neoprene wetsuit. (H) The composite material was attached to the suit in thinner neoprene pockets. The full suit was field tested. Source: [19]

The stiffer composite pieces provides an thicker thermal barrier to non-joint body features with large surface areas (e.g pectorals, abdomen, shins, forearms) while freeing the joint

areas (e.g ankles, knees, hips, wrists, elbows, shoulders) for flexible movement. Initially, different adhesives were tried to glue the composite directly to a neoprene wetsuit. Poor adhesion quality led to abandoning an adhesive process altogether. Instead, the composite pieces were glued into two mm neoprene pockets and attached onto the base wetsuit.

In field testing, the ΔT between the inside of the suit (near the heart) and the ambient water temperature was measured with continuous data loggers, shown in Figure 2.11.

Figure 2.11. Synchronous Data Loggers for Field Testing Source: [18]

A single data logger was placed between the skin and the inner wall of the suit, nearest the heart. While this temperature measurement does not accurately measure the body's core temperature, it provides a reference of the temperature of the warmest water/skin region inside of the suit. Another data logger was synchronized with the other and measured the external water temperature and pressure outside of the suit. This data led to the calculation of ΔT used compare neoprene and composite suit performance.

Field tests were conducted with two different divers, one wearing a seven mm neoprene suit and another wearing the composite suit. These divers both had different body compositions. The temperature measurements between the two divers were compared to assess the difference in thermal protection between the two suits. Data in Figure 2.12 from a dive in [19] shows that the composite suit maintained a relatively constant ΔT throughout the dive, whereas the neoprene suit's ΔT decreased over time.

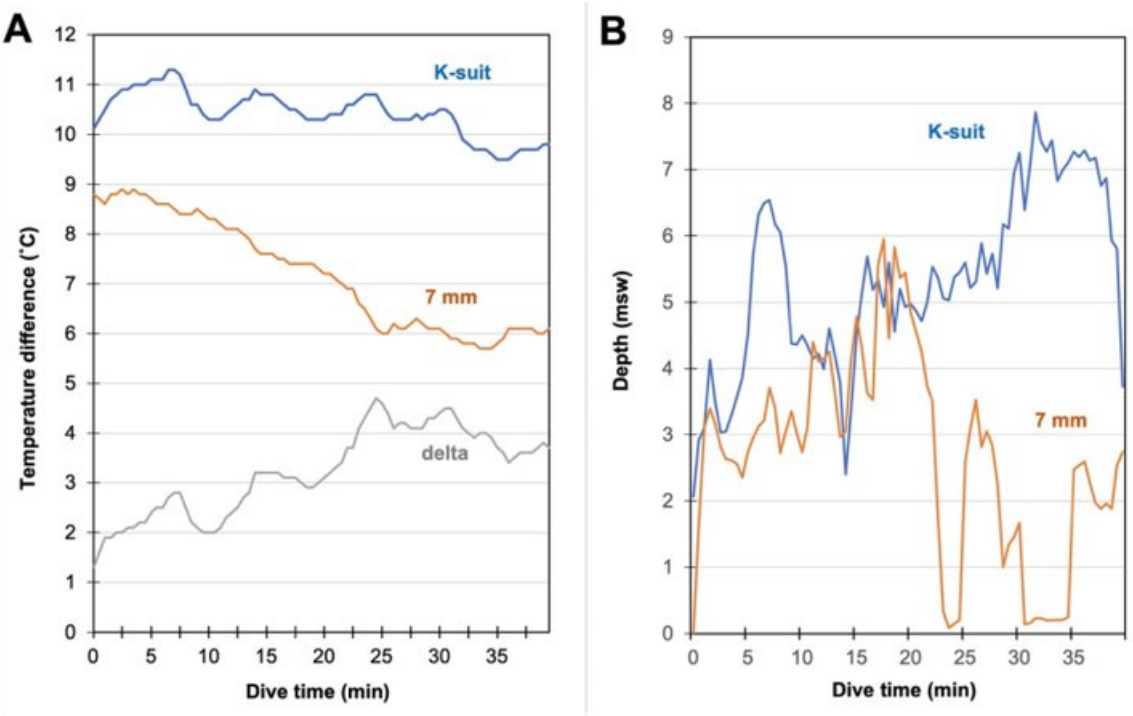

Figure 2.12. This field test supports the theory that incorporating stiff composites into a thinner neoprene wetsuits can produced comparable or superior ΔT results Source: [18]

After promising data from [19], a more aggressive coverage scheme with thicker paneling was attempted in Figure 2.13, to increase the ΔT between composite suits and neoprene suits. Improper sizing of the composite pieces in [18] led to repeated wear at the pocket seams. The uneven surfaces and dramatic features of the composite ripped the suit. Large pockets of water became trapped inside the suit and the thermal benefits were weakened, as the body could not warm the large internal volume of water.

Figure 2.13. The aggressive coverage scheme widened the composite pieces. Source: [19]

New prototype suits were designed to reduce the stress at wetsuit pocket seams and improve the fabrication process. A larger coverage scheme also makes the suit stiffer, contributing to poor fit.

2.4 Practical Challenges of Individual Casting

Practical limitations of an individual casting method also became more apparent with a larger coverage scheme. To accommodate these precise curved geometries, large deep molds were 3D printed. One mold was Three dimensional (3D) printed for every body feature. Excess material was hand drilled from vent holes in the mold. The mold's sharp angles, introducing the desired shape into the mold, also made it difficult to separate the mold lid from the bottom. Multiple screwdrivers were often used simultaneously to pry the lid from the mold. In some instances the mold lids cracked.

Designing the composite pieces before the base suit also creates difficulties in the fabrication process. The pockets were not symmetric in some cases, providing more or less coverage in different areas. The inflexibility of pieces also made fabrication difficult, as the material could not lie flat when being glued. Essentially, the suit was pinched into a single shape.

The individual casting restricted the flexibility of pieces in conforming to the diver suit.

The prevailing argument for individual casting is that these molds create composites with an exact representation of the scanned diver's body. However, these complex shapes are challenging to glue into a suit because of their preset curvature. Adding features to the composite pieces that allow flex in different directions may alleviate this issue. To have a larger coverage scheme and expedite the fabrication process, a more general approach can be taken.

2.5 Transition to Interchangeable Composite Pieces

The aim of future prototypes is to modify the tested composite material's surface geometry, drawn in Figure 2.14, to create an interchangeable fabric that is optimized to various curvatures. The schematic of the chocolate bar prototype shows features that will be altered during experiments to enhance the composites thermal performance for various curvatures.

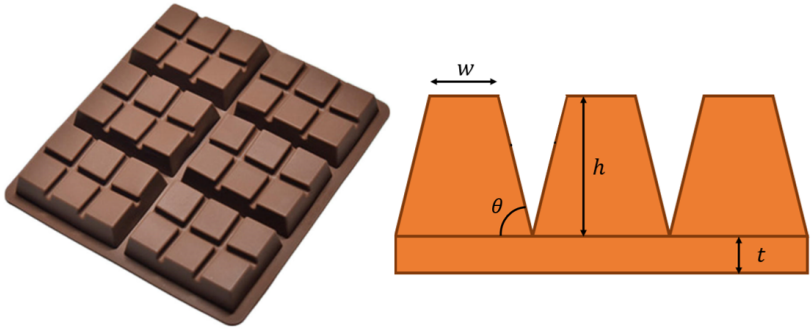

Figure 2.14. The envisioned prototype has similar characteristics to a chocolate bar shaped silicone tray. Source: [25]

The thinner sections of the paneling are intended to give the material more flexibility. Increased tooth height increases the thickness of the thermal insulation. Changing the tooth angle affects how well the teeth touch. Altering the base thickness affects the composites flexibility. In a similar way, an array of teeth, composed of composite material used in [21],

can be cast onto a thinner, more flexible base. The hypothesis is by adding grooves to the composite's surface (i.e a trapezoidal array) the composite may bend in multiple directions and conform to the diver.

Building the geometry in a simpler model, allows its features to be edited more easily in comparison to a constraining geometry from body scans. In this way more unique properties and shapes (e.g. pentagons, hexagons, cylinders, aquatic biology) can be rapidly modeled, cast, and implemented into a prototype. Bulk quantities of the composite material may be cured and cut to specific shapes, rather than using one mold per wetsuit piece. The universal cast can be applied to a range of body curvatures rather than a predetermined location as well.

Designing the composite as a flat piece that can be bent also reduces mold sizes and variation. Individual casting sets the curvature in the mold, with heights in the tens of centimeters. The envisioned mold for this new design is thinner, less than four centimeters, with the cavity occupying most of the printed space.

CHAPTER 3:
Experimental Methods

3.1 Custom Wetsuit Tailoring

A custom wetsuit tailor at Otter Bay Wetsuits in Monterey, CA was consulted to fabricate the composite wetsuit. Body measurements were taken to make a pattern for a three mm neoprene wetsuit base, diving hood, and 12 mm boots. The composite was incorporated at various body features by gluing it into thinner two mm neoprene and then gluing these pockets on the base layer with neoprene cement. A cross-sectional schematic of this design is shown in Figure 3.1 for a cylindrical body feature.

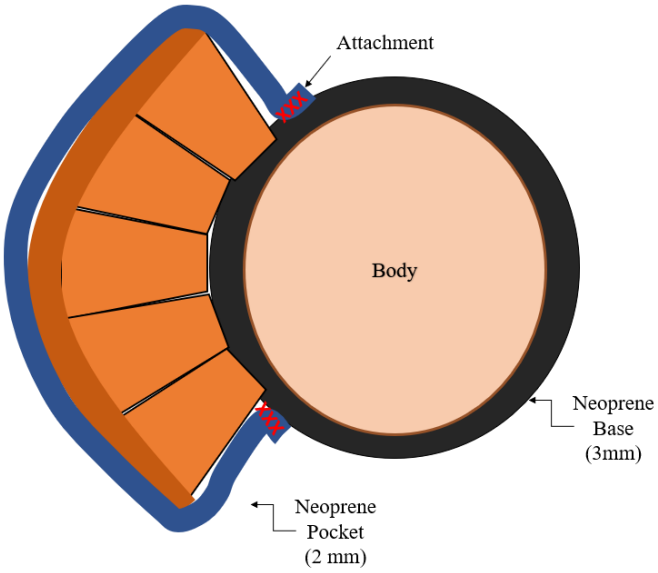

Figure 3.1. Ideally, when the composite is folded, the teeth touch each other.

3.2 Composite Coverage Selection

A series of measurements was taken with a soft tape on the base wetsuit to approximate a range of body curvatures. The Radius of Curvature (r) of cylindrical features (i.e., arms,

thighs, calves) was calculated from their Circumference (C) in Equation 3.1.

$$r = \frac{C}{2\pi} \tag{3.1}$$

For broader features like the chest and back, Arc Length (a) and Chord Length (c) were measured. The arc was measured as the span of soft tape between two pinpoints across the chest. The pinpoints were separated by approximately a 30.84 cm (12 in) chord across the chest. In some measurements, the chord length was varied, but this measurement was always the straight line distance between the two pins. The radius of curvature was iterated, such that the geometric relationship for the chord as a function of r in Equation 3.2 fell within 0.01% of the c measurement. The code used to determine these parameters is included in Appendix A.

$$c = 2r \sin \frac{a}{2r} \tag{3.2}$$

The resulting radii were arranged in a histogram to determine peak curvatures needed in the design. Two r values were selected to fit to high and low curvature body features. From these two r values, sample pieces were designed to cover a 150 mm curve (about six inches) with five teeth. From this basis, the Top Tooth Width (w_t) is constant for both molds. Assuming perfect contact between the teeth, the curve length is approximately the product of w_t and Tooth Number (N) in Equation 3.3.

$$s \approx w_t N \tag{3.3}$$

Body Curve Length (s) also can be defined as the product of r and Arc Curvature Angle (α) in Equation 3.4.

$$s = r\alpha \tag{3.4}$$

α can be divided by N into individual Tooth Angle (β) values in Equation 3.5.

$$\beta = \frac{\alpha}{N} \tag{3.5}$$

From triangular and parallel line relationships, the tooth's Tooth Draft Angle (θ) can be

calculated in Equation 3.6.

$$\theta = \frac{180 - \beta}{2} \tag{3.6}$$

With some additional trigonometry, w_t can be calculated.

$$W_t = w_t + \frac{2h}{\tan\theta} \tag{3.7}$$

Additionally, from a set offset and gap between teeth, the Outer Curve Length (S) can be determined with Equation 3.8

$$S = NW_t + (N-1)(\text{gap}) + 2(\text{offset}) \tag{3.8}$$

From these geometric relationships and assumptions the dimensions of composite pieces (w_t, Bottom Tooth Width (W_t), θ, and N) can be calculated. Base Thickness (t) and Tooth Height (h_t) are defined based on previous prototype thicknesses in [19] and [18]. These dimensions were used to model the flexible composite geometry for low and high curvatures. A schematic of all of these variables for two converging teeth is provided in Figure 3.2.

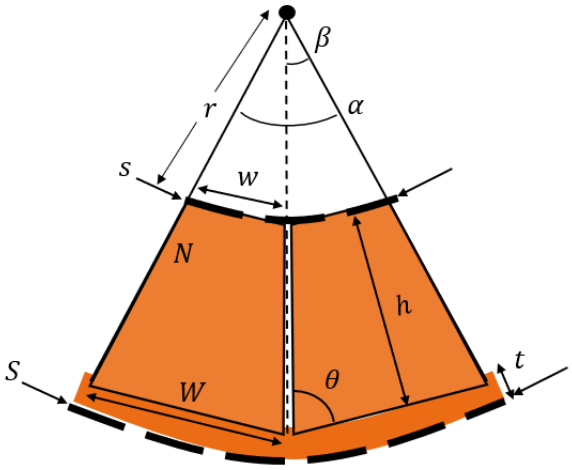

Figure 3.2. This schematic shows the necessary variables to design the composite shape for tooth convergence.

3.3 CAD Modeling

To model the positive geometry for the composite, a thin rectangular base layer was first extruded. Then a single square tooth was extruded from the base to the desired tooth height. With the draft tool, the tooth was sloped down to the base. This singular tooth geometry was then patterned across and down the base layer. These steps are pictured in Figure 3.3.

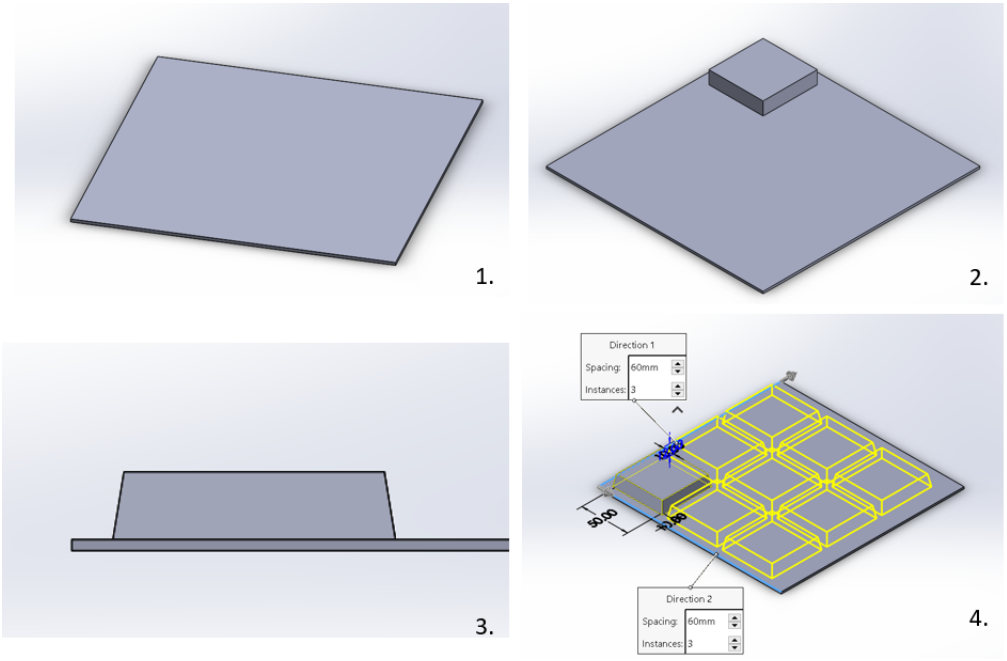

Figure 3.3. (1) A square base layer was drawn and extruded. (2) A single square tooth was drawn and extruded. (3) The tooth was drafted. (4) An array of equally spaced teeth was generated down and across the base layer.

Finally the base layer and the teeth were filleted at a 0.5 mm radius to create favorable lamination between the teeth and the base. The fillet angle was adjusted so that the individual teeth were close but not touching. Specifically, the spacing between the teeth was adjusted so that the fillets nearly converged. By this method the maximum spacing between the teeth was 1.0 mm. A sample of the final result, which was used as a template for other designs, is included in Figure 3.4

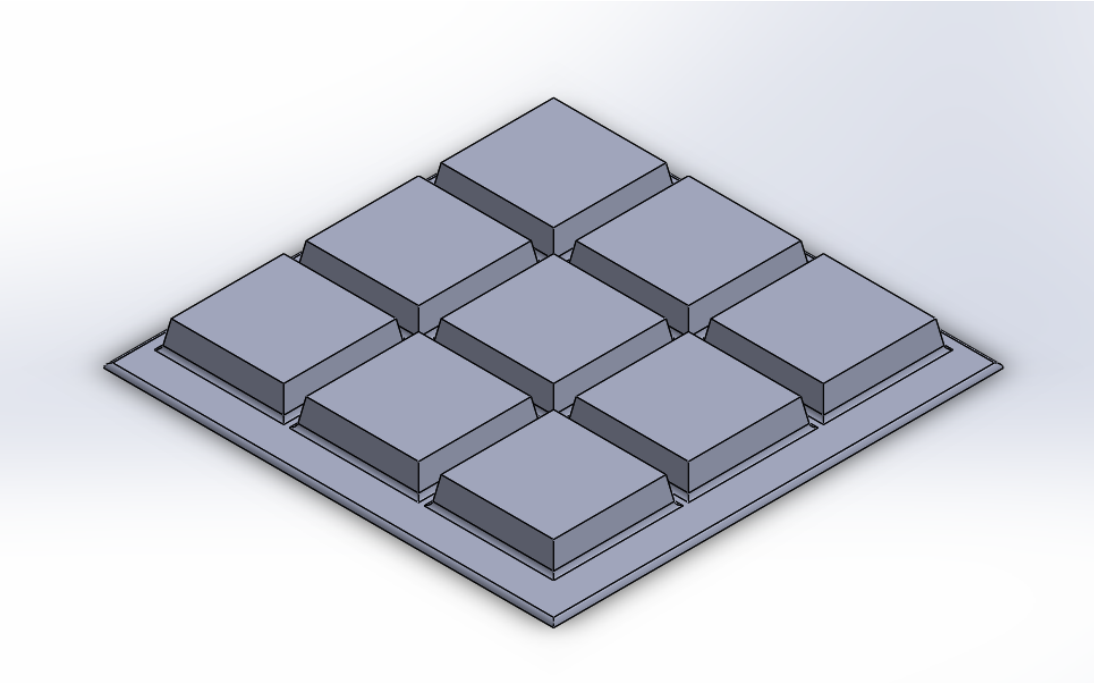

Figure 3.4. This template was modified to introduce new arrays of composite geometries and later produce their corresponding molds.

In a new assembly, the molds were developed from the positive model image. The mold was divided into a top and bottom section, where the bottom contained the negative image of the composite and the top was the lid. Note that changing features of the positive image does not automatically change the features of the negative image in the Solidworks software. In a template of the positive component, the tooth features and base thickness were altered and new molds were created for each prototype. To create each mold, an assembly was created from the positive geometry. New parts were drawn within the assembly to create the mold top and bottom. First, the mold bottom was drawn as a prism from the rectangular perimeter of the positive image. Then, a cavity was inserted in the assembly, using the Solidworks mold tools. Once the mold bottom included the cavity, the new part file for the base was opened and edited. A larger lip surrounding the cavity was added to contain the lid. The inner mold perimeter was drafted so that the mold lid could be lifted more easily from the base. These steps are pictured in Figure 3.5.

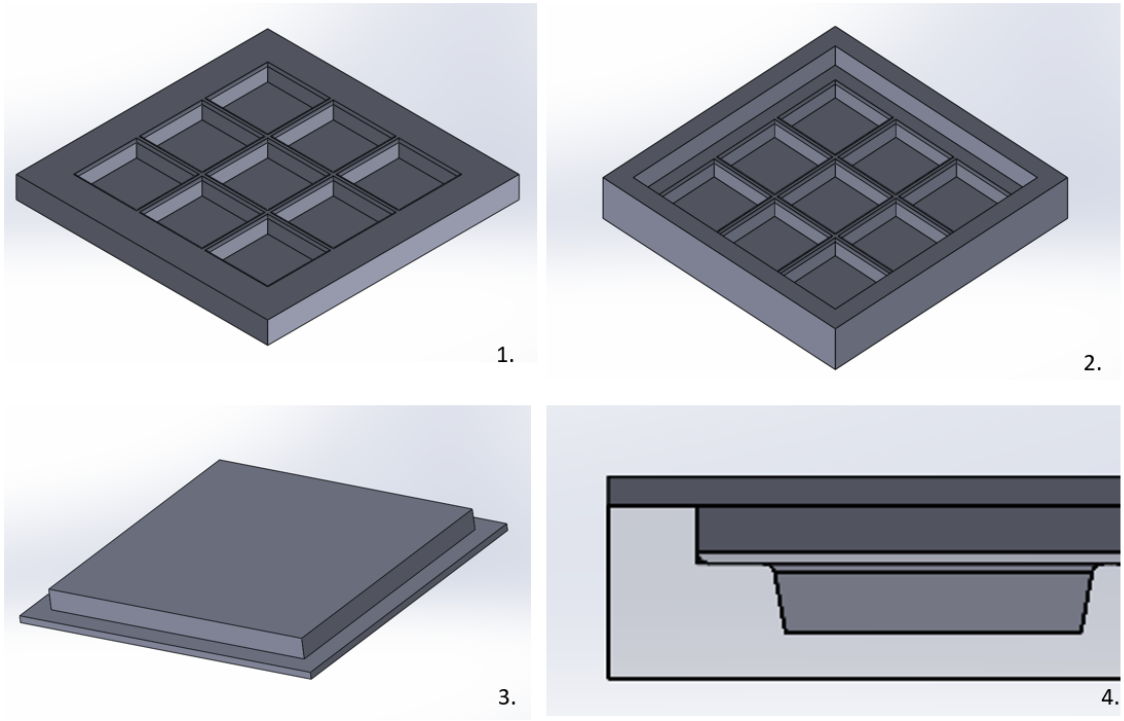

Figure 3.5. (1) A new part was drawn within the assembly and the cavity tool was selected to subtract the positive image from a square block. (2) An offset lip was extruded from the bottom mold to contain the molded surface. (3) The top of the mold was also drawn within the assembly and extruded from the surface of the positive image. The inner block filled in the remaining space in the bottom mold, and the top aligned with the bottom mold's outer edge to complete the lid. (4) A cross-section of the mold was examined to view how the bottom mold, the composite, and the top lid aligned.

Holes were added to the top mold to vent excess air from the composite during curing. Sample sizes of the molds with five by five tooth arrays were created for design development and thermal testing. The sample itself could be resized, by cutting along the grooves. Individual teeth could be broken from the sample as well for destructive mechanical testing. These sample molds were also large enough to create some wetsuit pieces, but eventually the mold design was expanded to develop bulk samples that could be cut and incorporated into a wetsuit.

3.4 3D Printed Molds

The mold components (top and bottom) were converted into STL files and sliced with Insight software. The parts were printed in solid Polycarbonate (PC) on a Stratsys Fortus 450mc 3D printer (Figure 3.6) with a T16 extrusion tip, shown in Figure 3.6. Each layer had a thickness of 0.254 mm (0.010 in).

Figure 3.6. Stratsys Fortus 450 mc. Source: [26]

3.5 Composite Material Processing

After printing the molds, the composite material was mixed, cured, and poured. First, a two part Sylgard 184 Polydimethylsiloxane (PDMS) kit was mixed at a 10:1 mass ratio of elastomer to curing agent in a 300 milliliter (mL) plastic beaker. Hollow 3M K1 HGM, with a mean diameter of 65 microns [27], were added at a 3:2 volumetric ratio. The target mass formula was 9.00 g of curing agent, 90.00 g of elastomer, and 10.00 g of HGM. In a planetary centrifuge, given in Figure 3.7, the mixture was spun at 1500 Rotations Per Minute (rpm) for four minutes. Prior to spinning, the centrifuge was balanced by adjusting weights to the final mass. As precaution goggles, a disposable mask, and gloves were worn when preparing this mixture to reduce contact with the HGM. When handling the glass powder, the lab door and windows were left open for greater ventilation.

Figure 3.7. The Planetary centrifuge both rotates the mixture about the central axis of the machine and rotates the container at a 45 degree angle. This process ensures uniform mixing. Source: [18]

The final mixture was degassed in a desiccator to remove internal air bubble and was poured into the mold. Air bubbles from the containers were periodically vented to prevent overflow. Two degassing methods were attempted throughout the experimentation process shown in Figure 3.8.

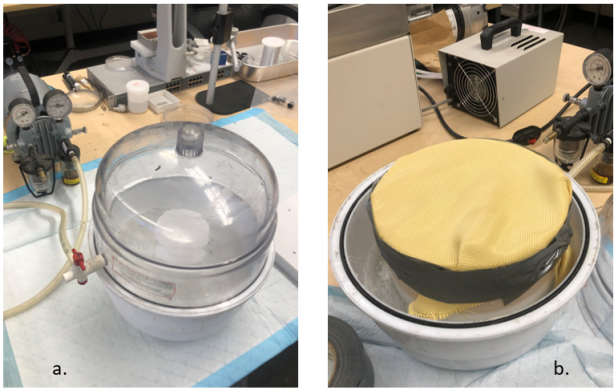

Figure 3.8. a) Original Degassing Setup b) Alternative Degassing Setup

The original method degassed the mixtures in their individual beakers. The beakers were later mixed in the mold. The alternative approach first mixed all of the containers and then

degassed the mixture in a wider bowl. To prevent overflow while still allowing air to escape, a porous cloth was taped to the top of the bowl. The composite was poured into the molds, and the excess was squished out by pressing the top and bottom together. Maintaining firm even pressure on the lid was key to reducing the reintroduction of air into the composite. To prevent the lid from buckling, the edges of the top mold were secured to the bottom with either clamps or bolts (depending on the mold design). Then, the composite was cured in an oven at 26.67 °C (80 °F) for two hours. Once fully cured the composite was removed from the oven, left to cool, and removed from the mold. Excess material from the vent holes and edges was cut from the composite's base with a razor blade or scissors.

3.6 Examining Porosity

The porosity of composite samples, prepared with the previous and alternative degassing methods, were compared under a SF-2TRA Stereo Zoom Microscope, given in Figure 3.9.

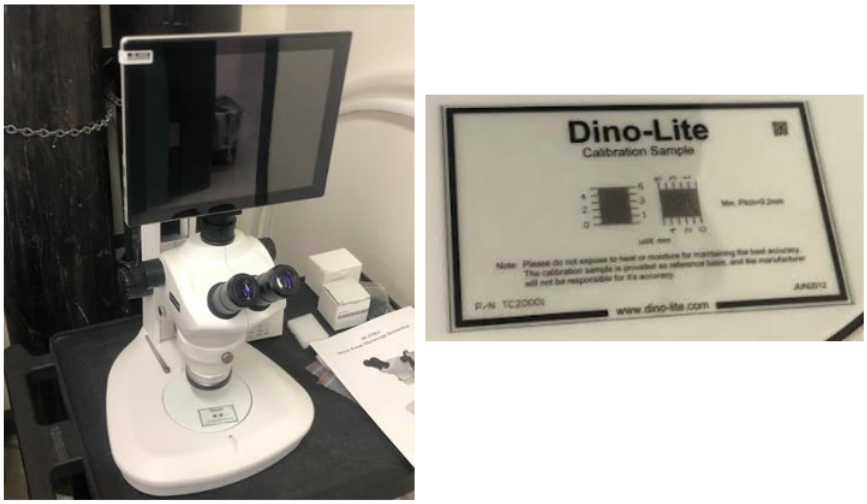

Figure 3.9. SF-2TRA Stereo Zoom Microscope

Thin slices of composite from the tooth array were cut vertically from the base to the tooth tip. A sample from previous wetsuit prototypes, a sample from early prototyping of the flexible composite concept, and a sample with the alternative degassing method were both examined. A thin transparent film with a millimeter scale was laid over the sample,

and the microscope was focused on the composites features. The pore sizes from all three samples were measured and compared in histograms with ImageJ software. These porosity measurements were used to later quantify the impact of porosity on Θ measurements of the composite material.

3.6.1 Mechanical Properties of Composite Samples

Compressive tests were conducted to compare the allowable stress of the composite material with high porosity versus low porosity. This testing was used to quantify the effects of an alternative degassing method.

The Bluehill 2 software on an Istrom machine measured the compressive force (F) of the sample and the extension of the loading cell, corresponding to the deformation (δ) of the sample. These measurements were converted into stress and strain by accounting for the sample's average cross-sectional area and height, shown in Equation 3.9 and Equation 3.10.

$$\sigma = \frac{F}{\bar{A}} \tag{3.9}$$

$$\epsilon = \frac{\delta}{\bar{H}} \tag{3.10}$$

The samples were cut from individual composite teeth. The sloped features of the teeth were trimmed, so that the whole sample had a uniform rectangular cross-section.

3.7 Optimizing Flexibility

Several samples with different thicknesses were produced to determine the right base thickness for a homogeneous composite with desirable flexibility. Four separate lids that produced base thicknesses ranging from two to five mm were 3D printed along with each base mold. The lids were sized so that they could be interchangeable for the same mold bottom. The flexibility of the cast composites was visually observed. For these samples, h_t was kept constant at 10 mm.

3.8 Experimental Insulance at Designed Curvatures

To measure each composite's Θ at designed curvatures of 50 mm and 250 mm, metal jigs were machined from 6061 aluminum, 127 mm (5 inch) round stock to hold the composite's shape. The design plans for these jigs are included in Appendix C. A heater was placed on top of the jig piece and was warmed to 37 °C (98.6 °F), an approximation for core body temperature. The system was placed in ice water, approximately 0 °C (32 °F). The electrical power into the system was calculated from current and voltage measurements, integral to the controller. When the controller showed a constant heater temperature, current, and voltage the system was assumed to have reached steady state, and the resulting values were recorded. The key assumptions of this heat transfer experiment were:

- Steady State Heat Transfer
- Negligible Convection and Radiation Losses
- Fully Insulated Heater
- Cylindrical Coordinate System

With the known temperature difference across the composite and the known heat input into the system, the composite's Θ was calculated from Equation 2.14. A schematic of the experimental setup is drawn in Figure 3.10.

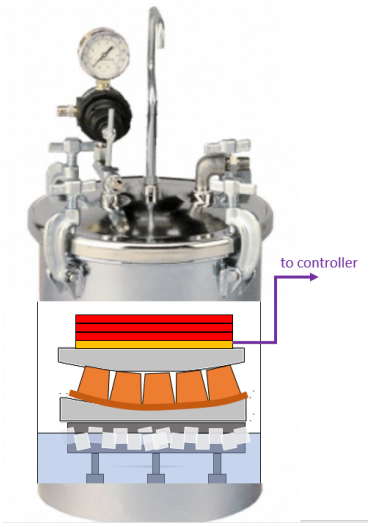

Figure 3.10. Thermal Properties Experimental Setup

The composite's Θ was derived from for a cylindrical heat flow, given in Equation 3.11.

$$q = \frac{S}{(H+r)\ln\frac{H+r}{r}} kL\Delta T \tag{3.11}$$

k can also be defined as the inverse of ρ,

$$k = \frac{1}{\rho} \tag{3.12}$$

or a function of Θ and Total Composite Thickness (H),

$$k = \frac{H}{\Theta} \tag{3.13}$$

Rearranging Equation 3.11 into Equation 3.14, the Θ for the curved samples is:

$$\Theta = \frac{S}{(H+r)\ln\frac{H+r}{r}} \frac{LH\Delta T}{iV} \tag{3.14}$$

The Θ values of each composite were first determined at atmospheric pressure in each designed jig. In subsequent trials, Θ was determined with increasing pressure, simulating increasing depth underwater. Finally, the Θ measurements in curved orientations were compared to Θ of flat puck HGM composites in [21].

3.9 Incorporating the Composite into a Diving Wetsuit

Once all necessary material was assembled, the cast pieces were laid on the diver, wearing the suit. Pockets were tailored by outlining the pieces on the body with a mica pen. Two mm neoprene pockets were cut to these drawn shapes on the suit. The flat base of the composite material was glued to the neoprene and then sewn into the base three mm material. The process of tailoring the composite pieces to the neoprene base is illustrated in Figure 3.11.

Figure 3.11. A composite piece is laid out on the thigh and traced by a custom wetsuit tailor.

3.10 Dive Testing

The fully fabricated suit was field tested at San Carlos Beach in Monterey, CA. As done in previous field testing, temperature and pressure measurements were continuously measured throughout the dive for two divers using synchronous data loggers. However, data in these experiments was only collected for one diver. This decision was assumed to eliminate the variance in temperature difference due to body composition between divers. As noted in [14], conduction through subcutaneous tissue of immersed bodies can reduce heat transfer by a factor of 15. Regardless of this assumption between data sets, height and weight were noted to make a fair comparison to ΔT results in [19]. The height and weight of the test subject was 195.58 cm (6 ft 5 in) and 93 kg (205 lbs).

Notable changes in the suits appearance, observations about performance characteristics (i.e. flexibility, thermal protection), and circumstances that may have led to poor or greater thermal results were documented. A summary dive log, including max depth, bottom time, starting and ending tank pressure were tabulated.

Initial dive testing was done with a full neoprene suit, specifically a BARE 8/7 Velocity Ultra Semi-Dry Wetsuit (Figure 3.12) rented from Bamboo Reef dive shop.

Figure 3.12. BARE Wetsuits are outfitted with OMNIRED Infrared Technology, which claims embedded minerals within the suit reflect radiated heat back to the diver. Source: [28].

For safety, diving was conducted with a dive buddy and in favorable sea states, with low current, wind, and swell conditions. Dive locations were chosen on recommendation from local divers. All dives were conducted near San Carlos Beach in Monterey, CA. The table and schedule of the dive plan were recorded. The beginning and final air tank pressure was recorded following each dive.

Air tanks were filled and inspected by Aquarius and Bamboo Reef Dive Shops. Extra equipment including fins, regulators, gloves, boots were either rented or purchased.

3.10.1 Diving Instrumentation

Over the course of the dives, depth in meters of seawater (msw) and temperature in °C were tracked with OMEGA OM-CP-PRTEMP1000 gauges. The gauges were attached to the inside wall of the suit, near the sternum. This temperature reading was a measurement of the water film temperature inside the suit. Though an inaccurate representation of the body's core temperature, this temperature is assumed to be the relatively warmest region within the suit nearest the heart. A line was tied through an eyelet in one gauge and worn around the neck, while the other gauge was secured in the pocket of the Buoyancy Compensator (BC).

Pictures of these gauges are shown in Figure 3.13.

Figure 3.13. Dual Synchronous Temperature and Pressure Gauges: (left) the gauge placed inside the suit, worn around the neck (right) the gauge outside of the suit, attached to a ringlet on the BC

Prior to dives, the data loggers were activated using OM-CP Data Logger Software. The start time of the dives were synchronized by delaying the start to the approximate arrival time to the dive site. The data logger was manually stopped using the same software. Note that connection to an internet network is required to start data loggers. The resulting data was downloaded to an Excel file. The dataset was trimmed to filter the time that the diver was immersed in water.

Observations about the suits fit during each dive were noted. Changes to the suit after diving were written, and design recommendations were made in consultation with more experienced divers for future work. Additional tailoring alterations were made to correct any suit deficiencies and add protection. New designs iterations were tested again by the same method.

Plots comparing the temperature difference between the two gauges were compared to the diving depth pressure data. All dives were plotted on the same graph to compare field results.

THIS PAGE INTENTIONALLY LEFT BLANK

CHAPTER 4:
Results and Analysis

4.1 Design Progression

The design of the flexible composite architecture and wetsuit progressed in multiple phases. The first phase established a template architecture model that could adapted to a range of body curvatures by changing the tooth's draft angle. Then, sample pieces of the material were produced and were visually, thermally, and mechanically characterized. This design process culminated in the production of a composite wetsuit that was field tested in a real salt-water environment, pictured in Figure 4.1.

Figure 4.1. Pictured are the front of the suit (left), the back of the suit (middle), and a squatting position to show the suit's range of motion (right). The thin sections at the joints allowed for full arm and shoulder rotation, much like a surfing wetsuit. The composite wetsuit was noticeable heavier than the neoprene wetsuit, but about five extra pounds were needed to counter the added buoyancy of the composite paneling.

4.1.1 Body Measurements

To start the design process, soft tape measurements were converted into radii of curvature and arranged in a histogram, given in Figure 4.2.

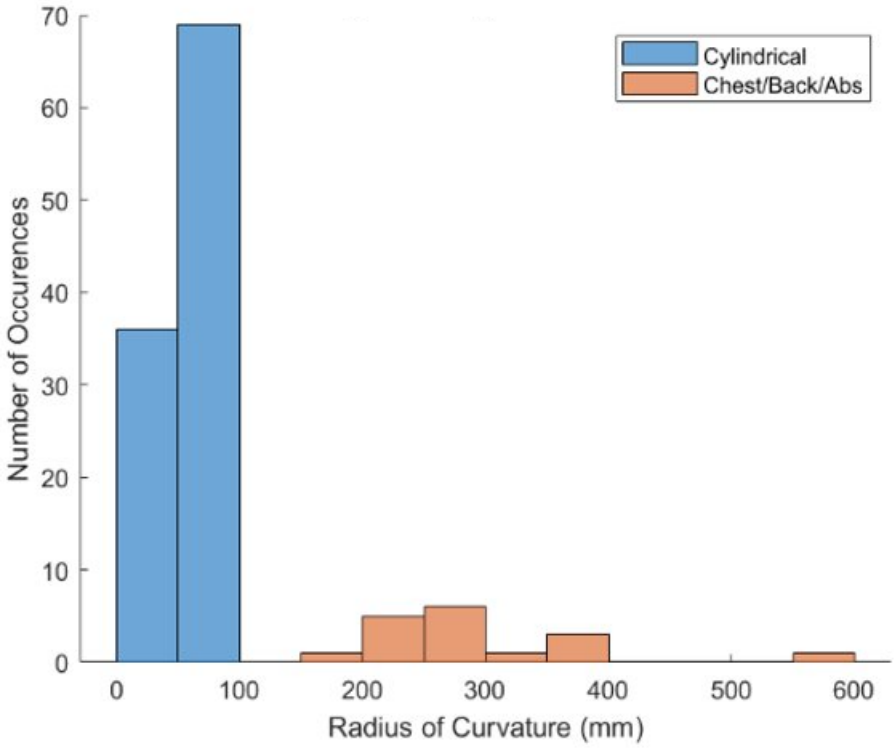

Figure 4.2. Histogram of measured radii of curvatures for cylindrical and broad body features

From the bimodal distribution, the two radii selected were 50 mm and 250 mm. These values were about a standard deviation below the two mean values of the bimodal distribution. Conceptually, a lower radius of curvature has a more cylindrical shape. Large radii appear more like flat surfaces. A scatter plot of the curvature data is represented in Figure 4.3.

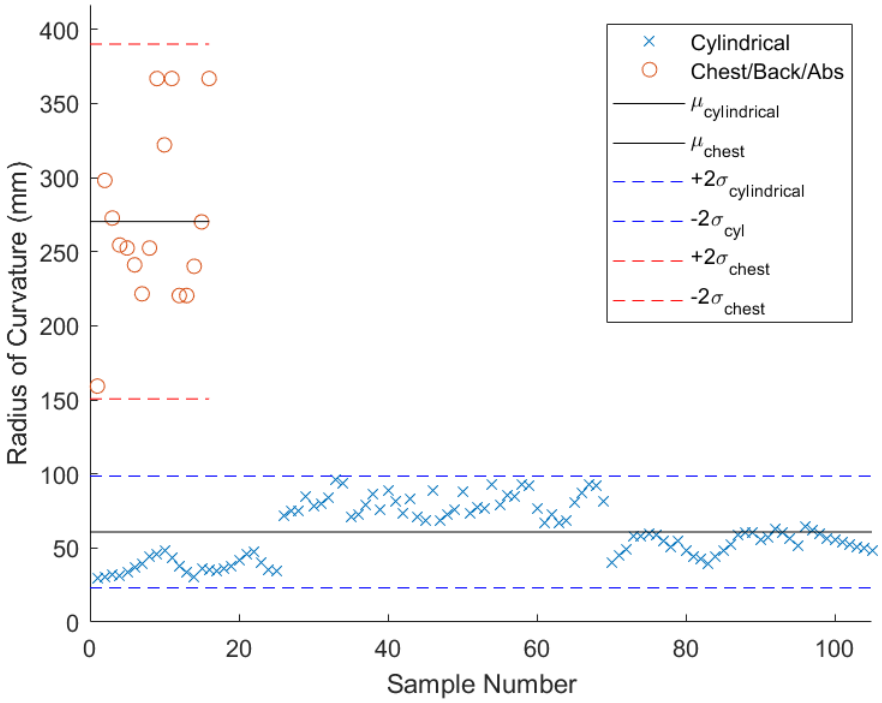

Figure 4.3. A scatter plot of the radii of curvature showed two distinct groupings of curvatures. Values below the mean were selected in order to cover a majority of curvatures in the grouping.

Selecting a design radius of curvature on the higher end of the distribution limits coverage due to over compressing the teeth. By selecting a lower end of the distribution of curvature, the teeth can open up to cover more body curves. Constraining the design to two radii was decided to limit the scope of the project. This data was also specific to one body. In future experiments and prototypes more radii of curvature can be tested. An ergonomic study of different body types may be helpful in producing body curvature distributions for specific sizes (e.g. small, medium, large).

Two corresponding molds were designed to accommodate these two selected r values. This design choice reduced the amount of CAD modeling that had to be done to create the pieces for the wetsuit. The prototype samples were designed in a five by five tooth array. In both models w_t was a constant 30 mm. The total area of the five by five array covered most

smaller body areas of the wetsuit design, spanning 150 mm (5.91 in).

4.1.2 Producing Prototype Samples

Multiple lids in Figure 4.4 were printed to vary the thicknesses of the composite samples from two to five mm.

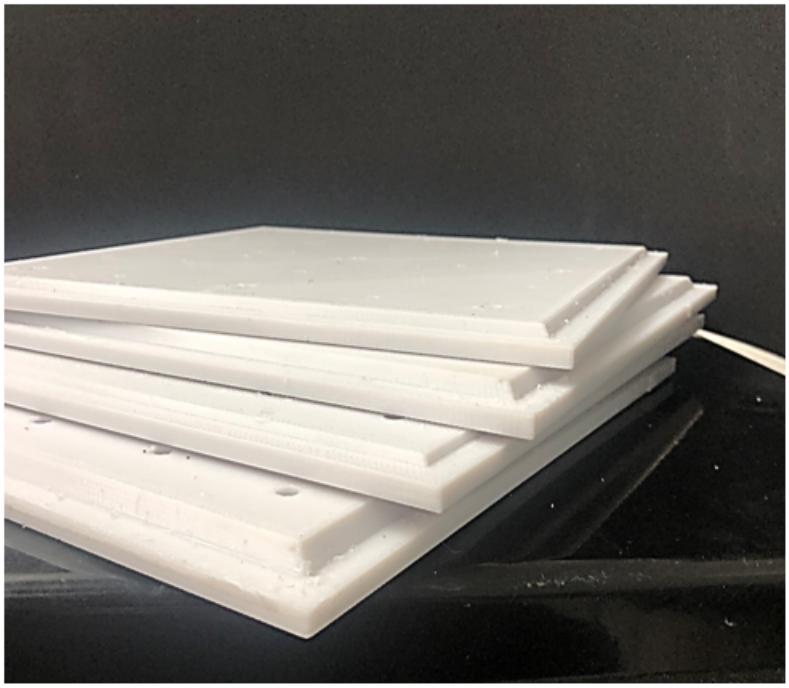

Figure 4.4. The thickness of the mold lid insert was changed to cast composites with different base thicknesses without 3D printing new mold bottoms.

Among the composites with various base thicknesses tested from two mm to five mm, all could be bent elastically to touch the teeth together. However, the amount of pressure needed to hold the composite in a curved position was greater for the five mm base compared to the two mm base. A composite with a three mm base and 10 mm showed consistent durability when removed from the molds and did not require considerable effort to bend as shown in Figure 4.5.

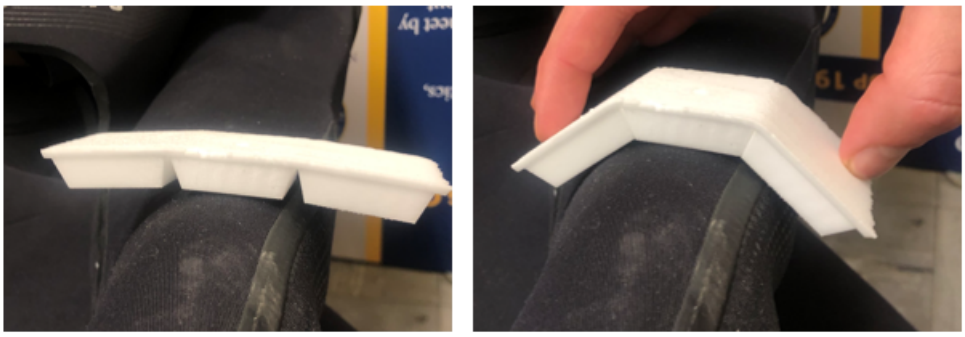

Figure 4.5. Unbent and Bent Composite samples on a dummy wrist

When laid over a body curve, the teeth converge when pressed together. Including a seamed pocket to hold down the composite in its curved position may provide the necessary force to keep in in place. Air may become trapped between the tooth gaps at imperfections. These teeth may provide a structure where larger volumes of air can become entrapped without compressing like pores. However, large opened grooves that can compress may result in weakened depth independence of the suit, like the air bubbles in neoprene foams.

The CAD designs in SolidWorks were designed so that the teeth when closed covered a 150 mm curve with five teeth. As a result the w_t was a constant 30 mm. For the two curvature samples, W_t and θ were calculated, while h_t was set to 10 mm, to improve the thermal insulation from previous prototypes of about an eight mm thickness [19]. The specific design parameters used to create molds for the 50 mm and 250 mm radius of curvature are included in Table 4.1.

Table 4.1. Design Parameters

r	s	S	w	W	N	α	β	θ
mm	mm	mm	mm	mm		deg	deg	deg
R1-50	150	188.93	30	36.19	5	171.89	34.38	72.81
R2-250	150	3.38	30	31.20	5	34.38	6.88	86.56

4.1.3 Porosity Characterization

The first samples of the composite were visually porous at the surface. The remaining air bubbles following the degassing rose to the base during curing. The result was a high concentration of pores at the surface. The porosity near the tooth interface on the base material, made them susceptible to fracture. Figure 4.6 shows a dispersion of large millimeter sized pores from a thin tooth cross-section.

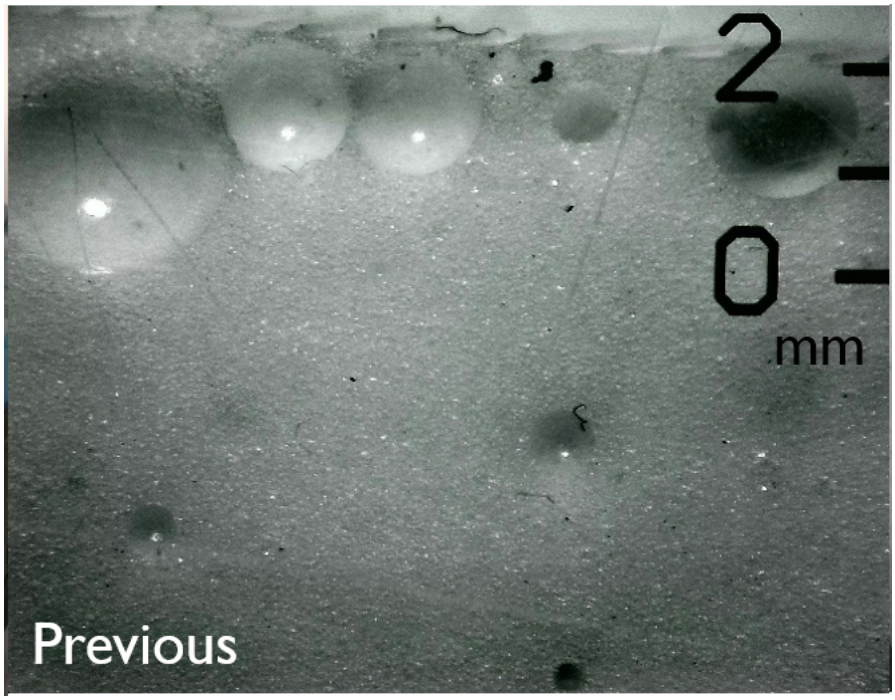

Figure 4.6. The high porosity in the initial sample allowed teeth to be easily broken. When bent the base experienced cracking as well.

In the first sample, the mold lid was not clamped to its bottom. As a result, the composite pushed up on the lid unevenly, creating a non uniform surface with large air bubble gaps. Additionally, squeezing the lid and bottom together repeatedly to try to get the tight fit, pushed air into the mold. The air coalesced into larger bubbles at the composite surface. To mitigate these effects, clamps were applied to the four corners of the mold, as shown in Figure 4.7. After overfilling the mold, the lid was laid on top. The clamps were slowly tightened in unison until the lid was fully pushed into the bottom.

Figure 4.7. The clamped assembly secured the lid in place as the composite cured in the sample size molds.

Applying the clamps required some coordination. The mold had to be lifted and held in place, as multiple clamps were hand tightened. Lifting the mold may have caused material to shift inside, creating areas for pores to form. Arc shaped patterns in Figure 4.8 of pores were visible on the composite's surface after removal. These shapes may be indicative of composite moving diagonally, when the mold was lifted to install clamps.

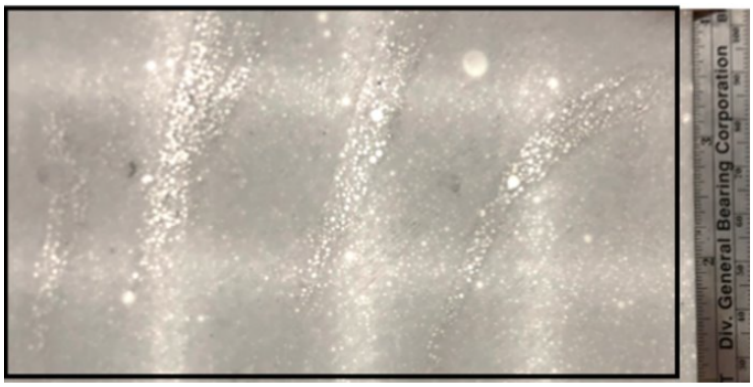

Figure 4.8. Pores appear to streak across the composite surface in large arcs.

As the mold is tipped to apply clamps, the composite folds over itself, creating these streak patterns. Despite efforts to secure the lid and firmly press it into the sample without

reintroducing air, porosity problems still persisted. The degassing method was the suspected source of the issue. Originally, once all the beakers were mixed individually, they were degassed in their own separate containers and mixed together in the mold. Folding multiple containers of composite into each other may have trapped pockets of air in the composite. To determine whether this problem was prevalent in other research, the porosity of HGM composites by individual casting were investigated to determine whether they contained pores as well. Optical microscope images confirmed the presence of similarly sized pores on a millimeter scale. These pores were able to be traced in ImageJ and arranged in a histogram, shown in Figure 4.9.

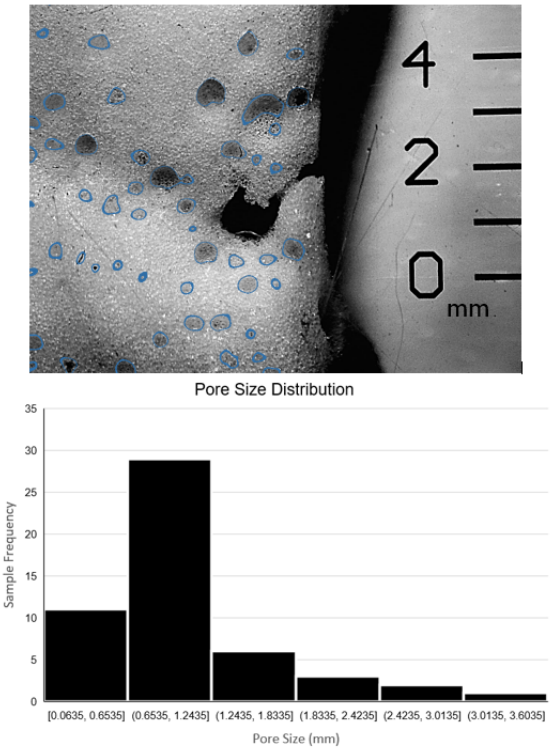

Figure 4.9. High Porosity Image J Tracing and Histogram

Within ImageJ, the image was converted to a 16-bit grayscale image. A bandpass filter was applied to discern which features were pores. A thresholding tool was used to pinpoint the distribution of the bandpass filter that outlined the pores. Pores were then traced with the

particle sizing tool and their individual perimeters were measured by the software.

To eliminate these large pores, the individual containers were first mixed in a large glass bowl and desiccated together as one mixture. The large surface area of the bowl allowed the mixture to spread and for more bubbles to reach the surface more easily.

Overflow from individual beakers was a concern in the previous method as well. Periodically, the air pressure of the desiccator would have to be relieved to prevent spillage. In the new method, the large bowl provided enough volume to prevent overflow. The vacuum could be switched on and the mixture could be left to desiccate for multiple hours. As a precaution to prevent overflow, a porous cloth was often placed over the bowl surface and taped around the perimeter.

Another strategy, which did not require a cloth or taping, was to fill the bowl to a low volume (in my experiments about four 300 mL beakers), let the mixture desiccate, stop the vacuum, add more a few more containers (up to nine 300 mL beakers total), and desiccate until no more air bubbles were visible on the surface. The entire degassed mixture was poured at once into the mold. The resulting reduction in porosity is given in Figure 4.10

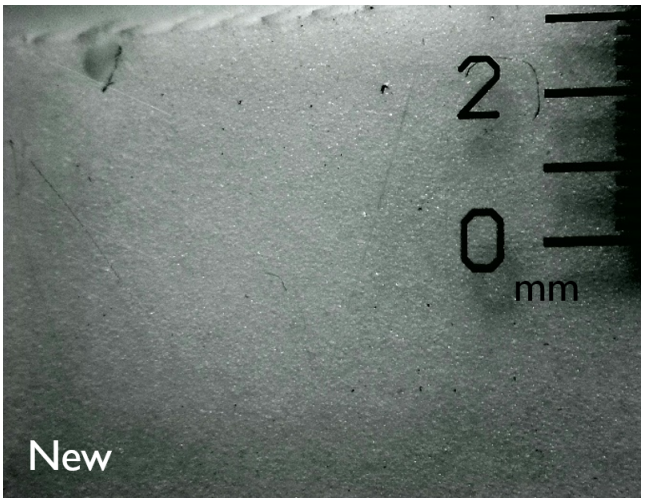

Figure 4.10. The improved desiccation method reduced the size of the remaining pores to a micron scale.

Image J software was attempted to be used to determine pore size. However, after a filter

and threshold were applied, the new pores were so small that they were confused with the individual microspheres.

Additionally, to improve mold lid placement, a bolt system was implemented to fasten the lid and the mold bottom together. This method may allow the mold to stay placed on an even surface, rather than be elevated and tipped to secure clamps. The bolts also forced the lid to stay level as it was pressed into the mold. The larger bulk samples were produced using a bolted mold, shown in Figure 4.11.

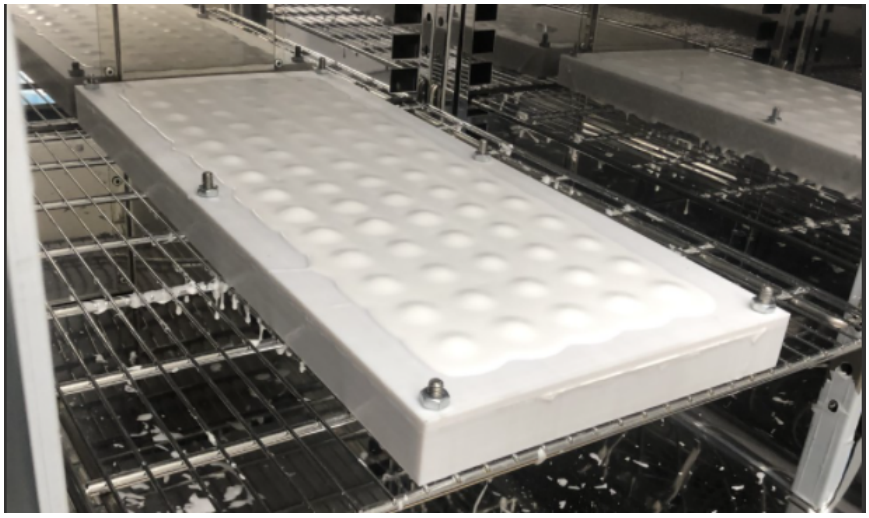

Figure 4.11. A larger mold included a bolted design that allowed the perimeter to be tightened more evenly.

The mold was enlarged to occupy the maximum length of the oven. The width of the piece was not adjusted, so that a realistic amount of material could be produced, degassed, and poured. Nine 300 mL containers were needed to fill this large mold.

To create greater ventilation of air bubbles during curing, more holes were drilled in the mold lid for each tooth. Having more holes also allowed the excess material to come out through the top rather than the sides. With more connections through vent holes, the composite stuck to the lid and was easier to remove from the mold bottom, as demonstrated in Figure 4.12.

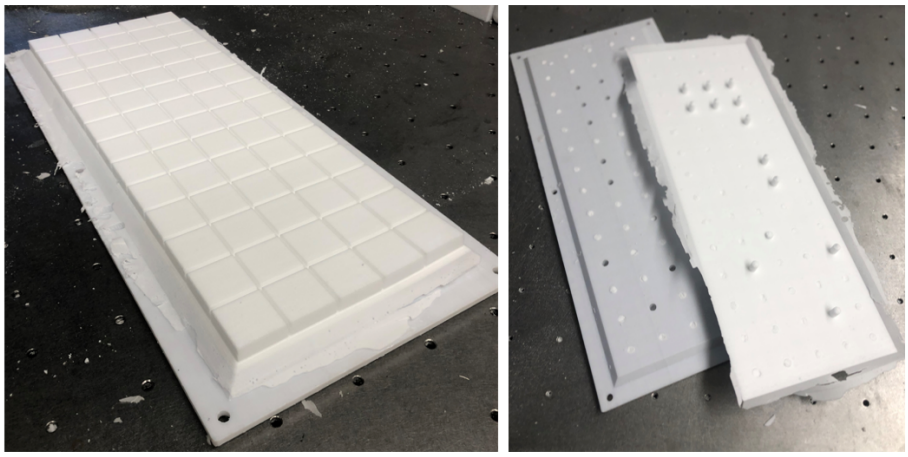

Figure 4.12. The excess material through the ventilation holes enabled the cast panel to attach to the lid surface and be easily removed from the mold.

This effect did not always work and was less effective for more porous samples. While the excess material is designed to be easily removed, these small features may be effective at lifting the cast piece out of the mold if they are stronger. The pore defects along with the stress concentration between the upright cylinder and the composite base create discontinuities, leading to their shear at the base. Adding a fillet around the ventilation holes may anchor the excess material better and improve composite removal in future work.

4.1.4 Compressive Testing

The mechanical properties of the HGM composite were further characterized in compression tests of uniform rectangular samples, prepared from individual teeth. A plot of the compressive stress v. strain of high porosity and low porosity samples is included in Figure 4.13. The sample was loaded on two different sides to determine whether it had isotropic mechanical properties

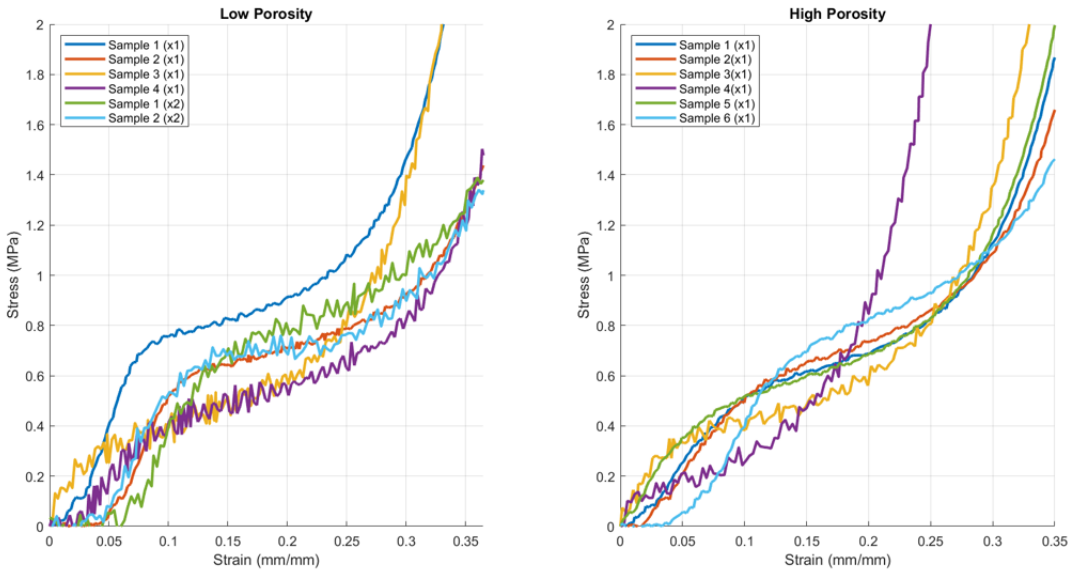

Figure 4.13. The inclusion of pores led to lower stiffness and yield strength to failure. These results followed similar stress-strain behaviors as discussed in [23] [24]

The stress-strain behavior of the HGM composite follows a similar sequence to other experimental results and compressive models of other HGM syntactic foams, discussed in [23].

First, the low porosity samples have steeper elastic regions because HGMs occupy the spaces within the carrier polymer that would otherwise be pores. Glass is a not only a stiff material, resistant to compression with Elastic Modulus (E) of 60 GPa and Poisson's Ratio (ν) of 0.31, but also it is a brittle material that deforms plastically for a wide range of stresses from 100 MPa to 10,000 MPa [23]. The inclusion of pores also are large surface defects that are the site of localized stresses to accumulate.

The plateau region has little to no influence on the stress-strain behavior of these experimental measurements. The data in all of the graphs transitions from the elastic region to densification. As the volume of the material is compressed, the HGM jam against each other, causing the internal stress experienced by the sample to grow rapidly. This behavior

occurs in the high porosity samples around 35% strain, whereas the densification region for the porous samples occurs earlier at 30% strain. In some of the porous samples, notably in Sample 4, yielding occurs close to the onset of loading. The transition in porous samples from the elastic region to the constant stress region occurs around 5% strain.

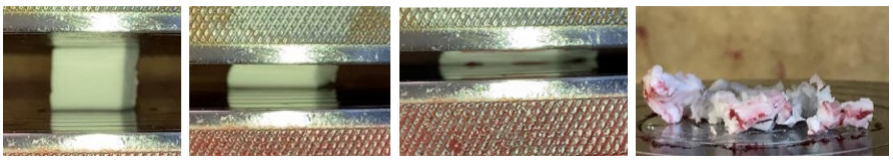

Figure 4.14. Progression of uniaxial compresion tests

4.1.5 Wetsuit Incorporation

With the larger molds, bulk samples of material were cast and tailored into the wetsuit, as shown previously in Figure 4.11 and Figure 4.12. This longer piece was expanded from an existing CAD template, using the same design parameters from Table 4.1. These large panels could be cut into multiple pieces by cutting along the groove lines. An example of this fabrication process is provided in Figure 4.15.

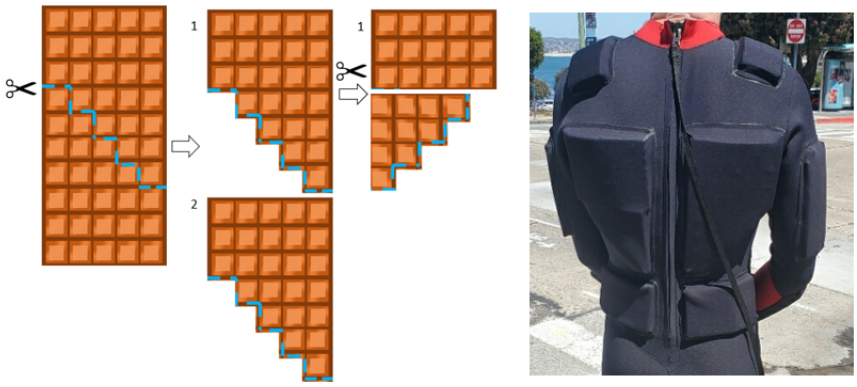

Figure 4.15. The composite pieces over the trapezius muscles were approximated as a trapezoids by cutting along a diagonal of a larger rectangular piece.

Cutting along the grooves was not limited to rectangular panels. In the case for the back pieces, the larger composite piece was cut diagonally, using a step approximation. This work allowed two large pieces, originally planned to be both rectangular, to be made from one. This design decision exemplified the utility of having a repeatable pattern. The chocolate can be cut to many approximate shapes allowed by the square grid. When cut on a diagonal, the two shapes were originally the same piece and not mirror images. To solve this issue, the sample was simply cut again, and a piece was reoriented to create a symmetric piece. This method reduced the need to make another large rectangular piece for the wetsuit. Instead, the material was optimized so that two pieces could be made from one. To fill the edge along the diagonal, triangular pieces of 12 mm neoprene were placed between the gaps.

To attach the composite to the wetsuit, thinner two mm neoprene pockets were produced to contain the composite shape shown in Figure 4.16.

Figure 4.16. Neoprene Pockets Containing Composite

The flat back of the composite piece was glued within the neoprene pocket using Neoprene cement. The flat surface of the panel provided an even surface area for the neoprene cement to be applied and dried. Once the piece was secured to the inside of the pocket, it was laid in its appropriate position. The edges of the pocket were glued to the neoprene base with the same neoprene cement. Multiple coats were applied to ensure a watertight around the pocket.

4.2 Thermal Testing Results

The Θ of the composite material at r of 50 mm and 250 mm were measured and compared with added depth. For each trial, the pressure was raised to a maximum of about 280 kilopascals (kPa) (40 Pounds Per Square Inch (psi)) and dropped in increments of about 70 kPa (10 psi). The corresponding diving depths for these pressures ranged from surface conditions to approximately 30 msw (90 feet of seawater (fsw)). A data point was taken for at each depth increment (once steady state was achieved) until atmospheric pressure was reached.

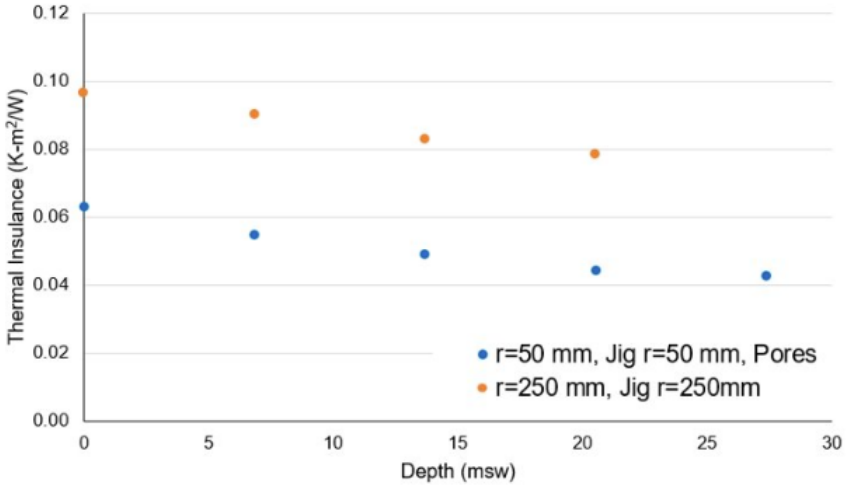

Figure 4.17. This plot graphs the Thermal Insulance of flexible HGM composites with depth for samples in their designed jigs, corresponding to their radius of curvature. A porous and non-porous sample were tested.

Despite the air gaps between the grooves, the flexible HGM composite had Θ values on the same order of magnitude as Θ measurements in [21]. However, the concavity of Figure 4.17 suggests that air compression does have an influence on the flexible composite's thermal results. Neoprene's Θ appears to have a higher concavity than the flexible composites; therefore, the influence of depth on the flexible samples is not as extreme. The lower porosity samples especially have a higher initial Θ, similar to the flat composite pucks, nearing 0.10 $\frac{Km^2}{W}$. For the porous flexible composite sample, the initial Θ started at 0.06 $\frac{Km^2}{W}$. This initial value is similar to neoprene's behavior in [21]. Neoprene also had a

lower initial Θ, compared to the composite puck. This difference may be attributed to the compression of the sample, bearing the weight of the heater or jig assembly. Reducing the porosity from the flexible composite samples impacted its thermal properties in addition to its mechanical properties, as previously discussed.

4.2.1 Challenges with Experimental Setup

The thermal properties measurements at depth were limited by the maximum allowable pressure of the vessel at 551.69 kPa (80 psi). Practically, the maximum working limit for SCUBA divers in wetsuits is 40 msw or 400 kPa (58 psi). However, a poor vessel seal made it difficult to measure pressure's above 275.79 kPa (40 psi). At this pressure the tank began to hiss as air escaped. The problem stemmed possibly from a worn gasket between the lid and the pressure pot. The inner drum appeared to be cut with scissors as well. Corrosion was also noticed on the bottom of the pot as well but was not investigated further for its possible contribution to leakage. Eventually, the pressure pot was replaced.

Another challenge with the experimental setup was waiting for the system to steady without a time measurement. A computer software may be a helpful addition to determining when the system actually steadies. With a longer wait time, the ice within the pressure vessel has more time to melt. Once a series of measurements is completed, (i.e. starting at high pressure, decreasing at an interval, and ending at atmospheric pressure), if the ice is melted, then those thermal measurements are invalid. At that point we do not know when the ice melted. Having a thermocouple in the water, may also be a good addition to actively track the temperature of the water inside the pressure vessel. Assuming ice water has a 0 °C simplifies calculations and setup, however, this assumption can only be confirmed with the a visual of ice at the start and end of each trial.

The seal of the pressure vessel was an issue. Above about 280 kPa (40 psi), the vessel began to continuously hiss and the larger compressor started to make up the lost pressure. Introducing pressurized air continuously into the vessel may have caused forced convection around the jig apparatus. Below 280 kPa (40 psi) the seal consistently held the internal pressure.

A temperature measurement of the surrounding air in the container may also be a good addition to the experimental setup. Without visual of the samples in the pressure vessel and

with only P_e measurements for feedback, makes it difficult experimentally to pinpoint any inconsistencies in the data. Tracking the controller's temperature with a computer software that records time may be a better method to determine whether the heater is reaching a steady state.

4.3 SCUBA Dive Field Testing

The fully fabricated suit was finally field tested in a seawater environment. All dives were conducted at San Carlos Beach in Monterey, CA. Temperature measurements were only taken for one diver and one suit for each dive. The temperature measurements of a dive buddy were not taken due to a large visual disparities in body composition. A dive log noting the max depth, bottom time, and starting and ending tank pressure is included in Appendix D. Individual plots of the temperature difference and depth data were included with observations of suit performance for each dive. A compilation of all recorded temperature differences and depths was finally compared on the same graph. Diver feedback on suit design and significant observations about wearing it were recorded. Feedback from local diving professionals was also considered.

4.3.1 Dive 1: Full Neoprene Suit, April 16, 2022

This SCUBA dive consisted of a series of repetitive dives to about eight msw. The entirety of the dive was spent reviewing basic diving drills. So, for the most part divers were stationary. Before each dive at San Carlos beach, divers enter the water from the beach. Then, they swim to a desired distance from shore, following markers along the pier. During the long surface swim, the ΔT data shows that the inner temperature steadied to approximately 22 °C. For reference this ΔT is 12 °C higher than that claimed by field tests of the NPS composite wetsuit in [19]. The BARE 8/7 semidry neoprene wetsuit worn in this experiment is advertised to reflect radiated heat back to the diver from "embedded minerals [28]." The inside of the suit wall is textured with fuzzy hexagon pieces as well, pictured previously in Figure 3.12. The BARE 8/7 wetsuit was a combination of seven mm and eight mm neoprene. The temperature and pressure throughout the first dive are plotted in Figure 4.18.

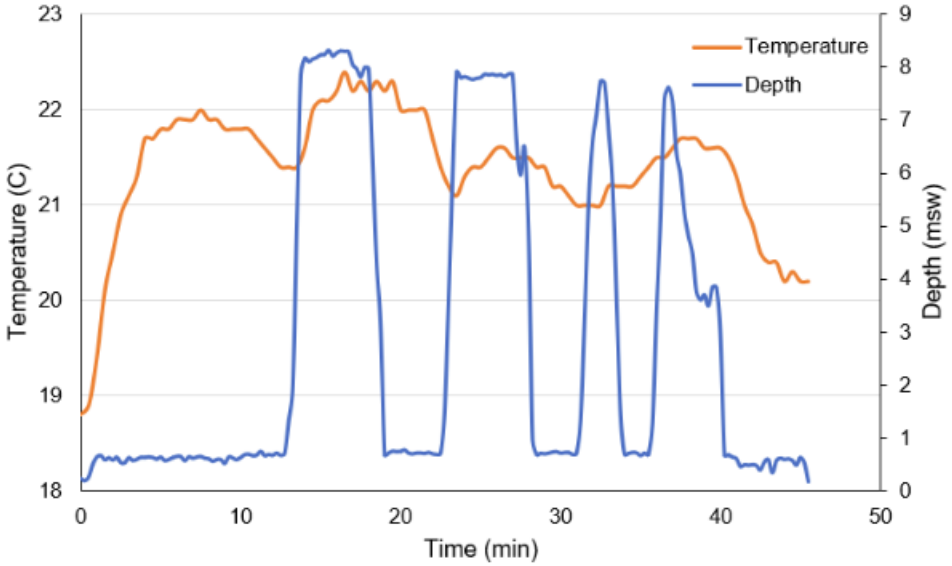

Figure 4.18. Dive 1: Neoprene Suit Temperature Difference with Depth

Donning the wetsuit was difficult to stretch over the shoulders. Often assistance was required. The suit opened from a middle zipper across the chest. This feature was especially difficult to close alone. While a dive buddy is essential for safety, the need to ask for help when putting on gear slows the process of actually getting in the water to do the dive. Despite these downsides, the suit felt very comfortable in the water. Referencing the data, the inner suit temperature stayed relatively constant. The integrated hood of the suit was also a nice feature that prioritized sealing around the head and neck area.

4.3.2 Dive 2: Full Neoprene Suit, April 20, 2022

The second dive was again conducted with the BARE 8/7 wetsuit, rented from Bamboo Reef Dive Shop. A similar experience was had in donning the suit as in Dive 1. The suit did not bend well. Help was often required, but in the water the suit felt very warm. These observations about temperature are consistent with the ΔT results, which stayed relatively constant throughout this dive. The temperature and pressure throughout the second dive are plotted in Figure 4.19.

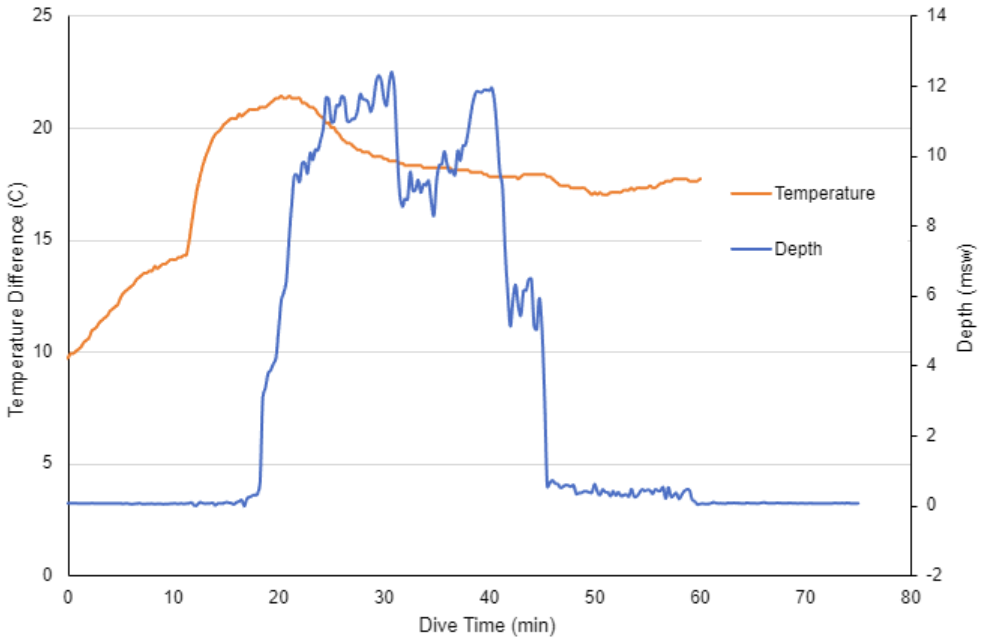

Figure 4.19. Dive 2: Neoprene Suit Temperature Difference with Depth

Kicking out to dive site from the beach was similar to Dive 1. However, the dive was a single dive, with a max depth of approximately 12 msw and a bottom time of about 25 min. From the bottom, the pierside was traversed to deeper water. Turning the head and neck is difficult in the thicker neoprene suit and hood. This was more noticeable because the visibility was particular great that day, approximately 15 m. Groups of sea lions and otters often approached throughout the dive. Greater flexibility at the head was also needed to better see a dive buddy. The googles block out peripheral vision, so the head must be fully turned.

4.3.3 Dive 3: Full Neoprene Suit April 20, 2022

As observed in previous dives with the neoprene suit, temperature stayed relatively constant, matching observations of a comfortable experience while immersed. This dive was conducted about thirty minutes after the previous dive. The temperature and pressure throughout the third dive are plotted in Figure 4.20.

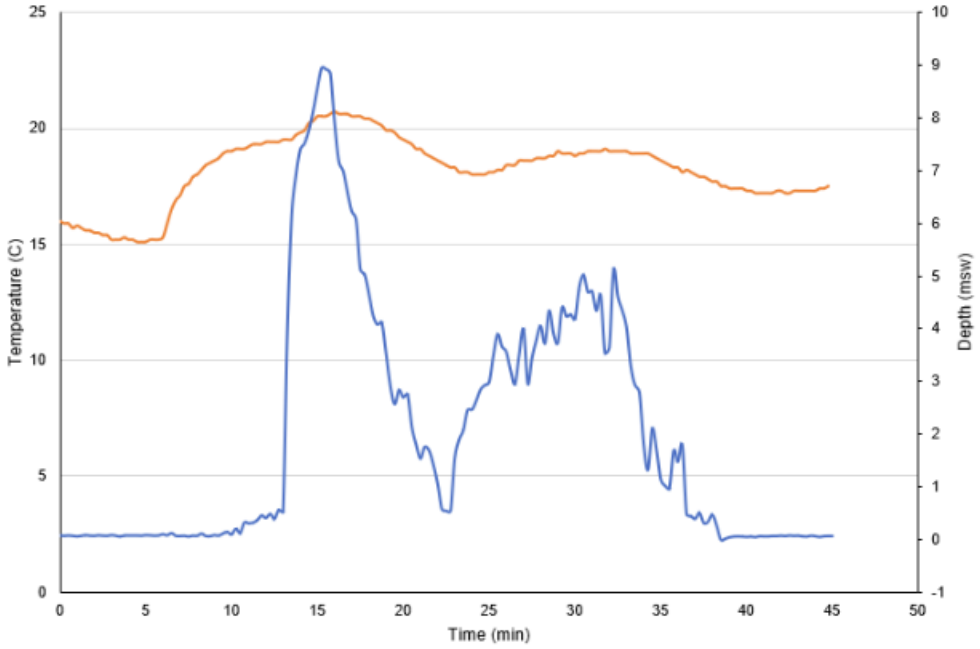

Figure 4.20. Dive 3: Neoprene Suit Temperature Difference with Depth

Following a return to shore, again the dive site was swum to from the beach. However, a shorter distance was swum to dive on a shallower kelp forest. With the variable terrain underwater in the kelp forest, buoyancy control is a concern. With variable depth a neoprene suit compresses and expands [8]. Going through the kelp forest required minor tuning to stay neutrally buoyant in the water column. The visibility was worse in the kelp forest, as the current and tide picked up more debris. Staying close to a buddy is important when traversing through the kelp forest. Entanglement in the kelp or losing a diver can be dangerous if alone. In this environment for dive buddies to stay close without interfering with individual passage through dense pockets of tall kelp.

4.3.4 Dive 4: Composite Suit, May 14, 2022

This dive marked the first time the flexible composite wetsuit was field tested. However, at this time only the body of the suit was prepared. The custom diving hood and boots were still being finished. Instead of wearing a custom hood and boots, a typical two millimeter MARE diving hood and SCUBAPro Boots were worn.

When donning the composite wetsuit, the pieces were initially flat inside the neoprene pockets, but as the suit was slipped on the composite conformed to the body as intended. The neoprene suit was just as easy to get on as a thin neoprene surfing wetsuit. The stiff composite pieces were often leveraged up the body to get the arms through the suit and pull it over the shoulders. With full flexibility the suit could be zipped without assistance from a dive buddy.

The custom pieces of the suit fit well, but the ready-made hood did not close an opening at the neck seal fit for the custom hood. The shorter draping could not be tucked into the wide opening. In effect, a large water pocket flooded the suit. This compromise in neck seal integrity is reflected in the rapid decrease of ΔT, shown in Figure 4.21.

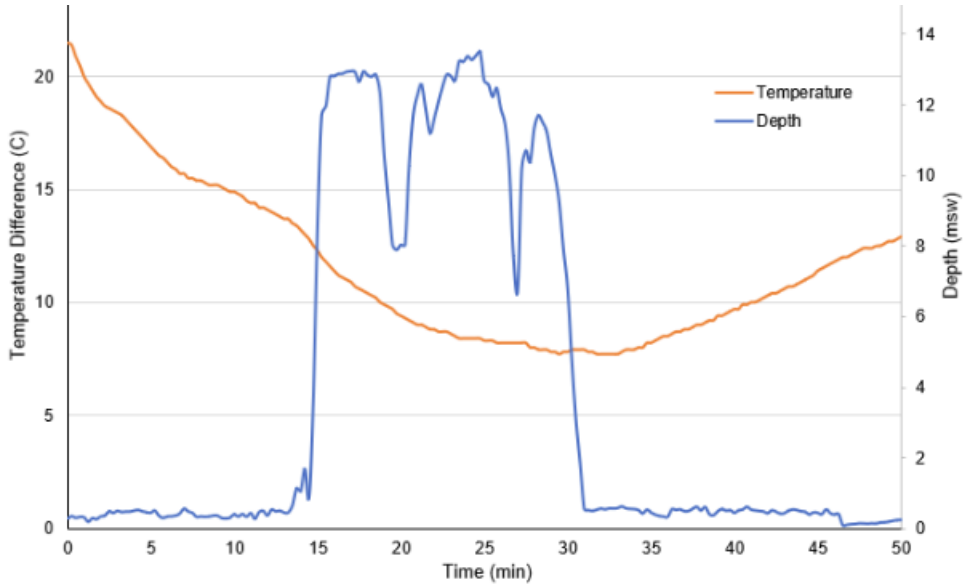

Figure 4.21. Dive 4: Composite Suit Temperature Difference with Depth

Initially, once neck deep water began to rush down the back of the suit. This felt shocking. Despite this compromise to the seal, the initial ΔT of the composite suit was near the superior neoprene wetsuit's performance. At the midpoint of the dive, the suit reaches a minimum at about eight degrees ΔT. At its worst, the compromised suit has a ΔT that is two °C less than the best of the previous composite suit in [19].

At a max depth of about 13 msw for 15 min, the composite suit did not perform as intended thermally. In terms of flexibility it was much easier to swim, kick, and look around. Once at the surface at the end of the diver, the temperature begins to gradually increase. This may signal that the body has adjusted to the cold water inside the suit, or it may be the result of some biological factor such as shivering. Once at the surface, shivering occurred, This shaking may have caused the water near the body to gradually warm up from agitation.

4.3.5 Dive 5: Composite Suit, May 14, 2022

A second dive was conducted in the afternoon, following the first dive with the composite suit. Divers from Cannery Row Aquatics were consulted as to how to improve the suit with a compromised hood. The shop graciously lent another hood, advertising the Waterproof H1 Diving Hood to be better quality and fit.

Despite a tighter fit, the new hood had a similar limitation in bib size. Like the MARE Hood, the Waterproof H1 Hood was difficult to stuff down the neck seal. As a result similar ΔT data was recorded, shown in Figure 4.22

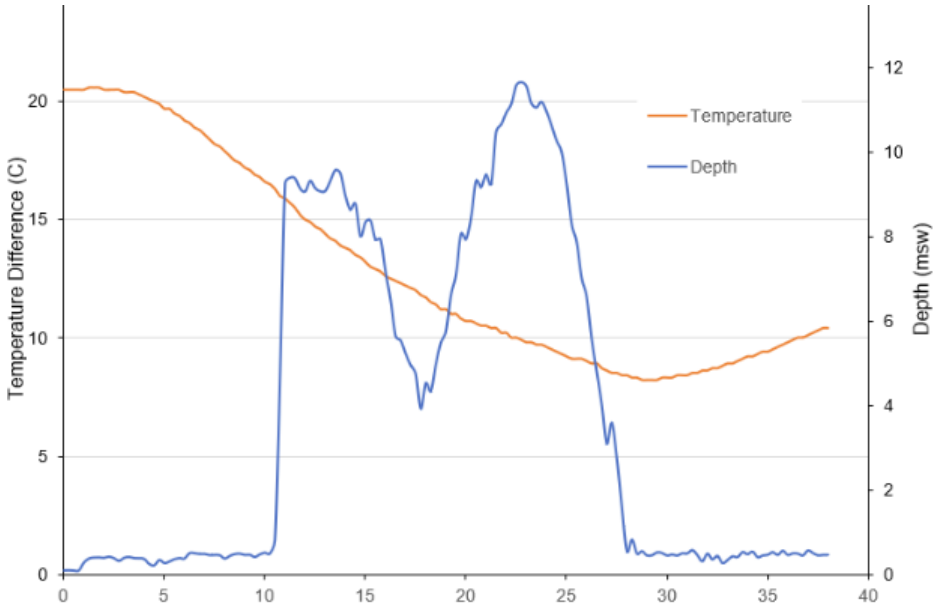

Figure 4.22. Dive 5: Composite Suit, Waterproof H1 Hood Temperature Difference with Depth

Similar to Dive 4, a rapid decrease in body temperature occurred with the compromised seal. ΔT only improved minutes after resurfacing. The time at which the temperature increased likely corresponds to the onset of shivering, which was also experienced minutes later after resurfacing while swimming to shore.

4.3.6 Dive 6: Composite Suit, May 15, 2022

Another dive test was conducted with the composite suit the next day; however, a malfunction with delayed start time on one of the data loggers resulted in no data collection for body temperature. Although there were no ΔT measurements, a similar experience occurred on the dive, while wearing the Waterproof H1 Hood again. This time the bib was not tucked into the suit as to not interfere with the neck seal. This dive was much longer than other previous experiments. However, the cold water inside the suit was not bothersome to abandon the dive. The water conditions were also colder than usual, around 48 °C. After surfacing, shivering began again on the swim to shore. The field test started again from the San Carlos Beach, but this time a farther swim was undertaken to reach the Metridium Fields dive site.

After removing the composite suit, the composite paneling was noticed to be broken on diagonals across the chest pieces, similar to the designed back. Additionally the abdomen and an upper arm piece were also broken at the groves. A suit pocket on the right chest piece was noticed to have opened at the corner. The full damage found on the suit is shown in Figure 4.23.

Figure 4.23. Post-dive Wetsuit Damage

The diagonal breakage across the chest paneling mirrors the designed cuts of the back pieces. This fracture may be a result of how the body is flexing the material. As an extension of future research, different coverage schemes can be attempted in new prototypes to correct common areas of breakage. After identifying these deficiencies, the suit was returned to Otter Bay Wetsuits for further inspection and repair.

The wetsuit grooves are repeatedly fatigued by flexing the suit to put it on and by actively wearing it. The composite needs to have the appropriate mechanical strength at the grooves to handle repeated stress. The grooves also act as a stress concentrator, where local stresses are much higher than the nominally applied stress. Reducing these stress concentrators by redesigning the tooth shape to minimize the groove may provide a solution in future research. Redesigning the teeth may also help increase the Θ of the teeth by reducing air gaps between the grooves.

4.4 Custom Hood and Diving Boot Fabrication

Following the repair of the wetsuit, the custom diving hood and boots were also finalized, shown in Figure 4.24

Figure 4.24. The custom diving hood and boots were finally completed to finish the entire suit fabrication process.

The hood was made of a three mm neoprene foam, while the boots were made of 12 mm neoprene. Unlike ready-made diving boots, these boots were slip on and did not have any zippers or Velcro. Both the hood and the boots were made from a custom pattern, measured during the initial tailoring process.

To attach treads to the bottom of the boots, four coats of neoprene cement were applied to both the tread surface and the sole of the boot. Once tacky the two pieces were pressed together from the toe to the heel. The edges of the tread were folded over the seams holding the boot sole to the upper shoe.

4.5 Full Custom Composite Suit Field Test: May 26, 2022

Once all of the custom pieces were assembled, the full composite suit was tested at San Carlos Beach in the early morning. The weather was damp and cold at the dive site prior to entering the water. The resulting ΔT measurements are given in Figure 4.25.

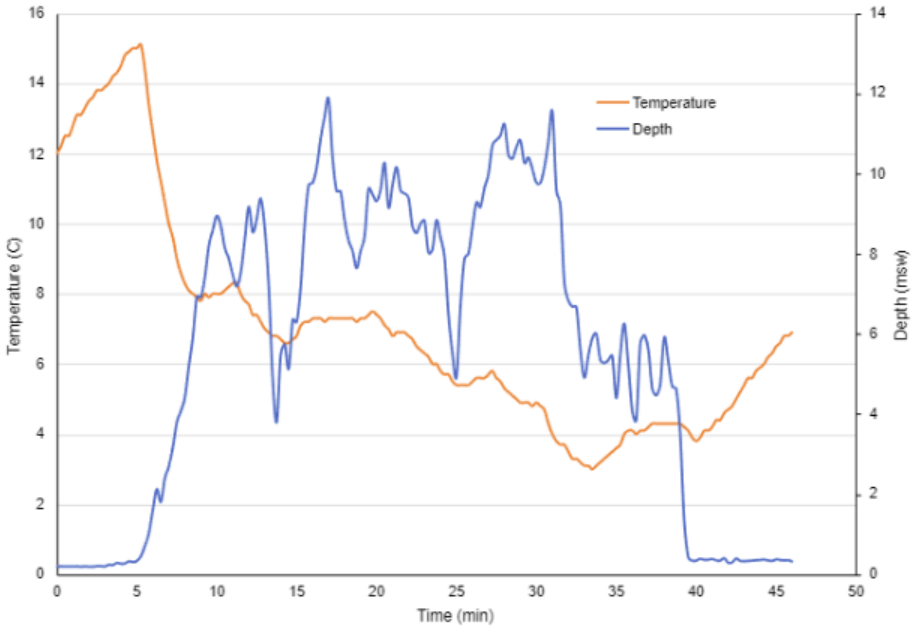

Figure 4.25. Dive 7: Full Composite Suit, Custom Hood, Custom Boots

Field tests of the composite suit showed severe thermal degradation to a low of three °C

between the surrounding water and the inside of the suit. Like previous composite tests, the suit again failed due to poor sealing. After putting on the wetsuit hood, the bib was able to tuck into the neck lining. However, the neck seal was still too loose and did not have a tight fit on the back of the hood. Water was able to surpass the hood and get into other parts of the wetsuit. Throughout the dive water squished in and out of the arms, legs, and neck. This circulation introduced a new layer of cold water into the suit. The weather conditions surrounding the beach were not pleasant. This colder air environment may have influenced the lower starting ΔT of 12 °C. The fatigue on the tooth structures may have also caused the suit to perform worse than expected. Determining better coverage schemes and strengthening mechanisms for teeth may improve this flexible wetsuit design in future research.

4.6 Comparison of Wetsuits

Although the composite suit's seal integrity failed, the ΔT results at their minimum are comparable to previous diving field tests. More dive field testing with composite suits and new prototypes are needed to accurately compare the fully neoprene wetsuit and the composite suit. A summary plot of all field testing experiments is included in Figure 4.26

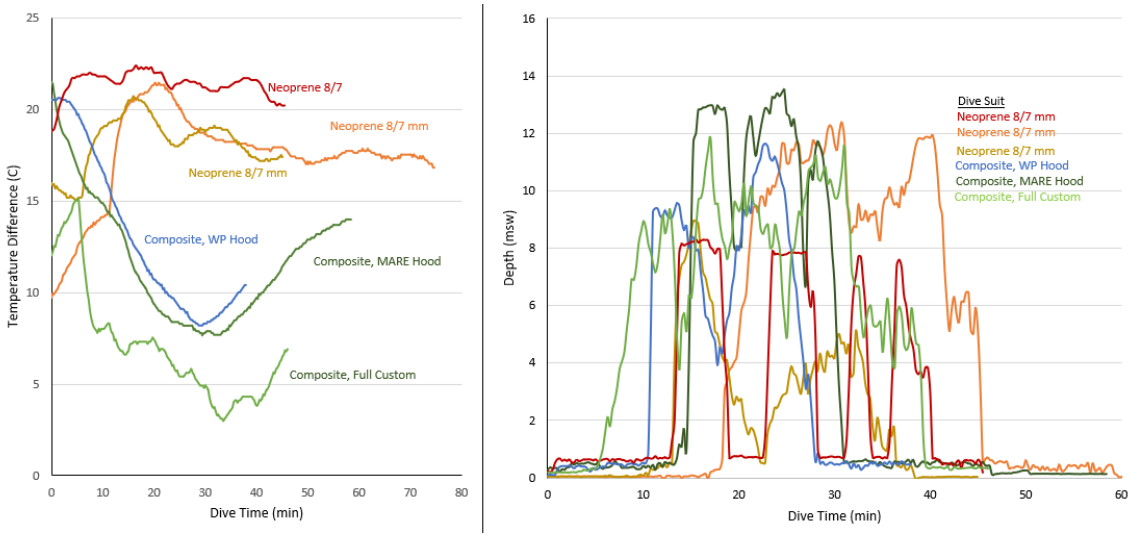

Figure 4.26. Summary of ΔT and depth measurements among suits.

An important consideration to reemphasize about the performance of the neoprene suit is that its performance is superior to previous composite prototypes by a difference in ΔT of approximately 12 °C and to previous neoprene suits by about 16 °C.

Additionally, despite the compromised integrity of the composite wetsuit's neck seal due to poor hood fitting, the initial ΔT for the flexible composite suit was near the advanced neoprene wetsuit. Graphically, the difference between the superior BARE 8/7 mm neoprene wetsuit and the flexible composite prototype suit is about 10 °C from the minimum of the composite performance to the steady state temperature of the neoprene suit.

The change in ready wear diving hoods did not improve heat losses. The large pocket of trapped water within the suit lead to rapid cooling followed by shivering on the surface.

Despite the weaker thermal performance of the composite suit, the ability to for the composite material to flex and adapt to body shapes is a milestone for this research and for incorporating HGM syntactic foams across complex geometries.

THIS PAGE INTENTIONALLY LEFT BLANK

CHAPTER 5:
Future Work

5.1 Recommendations for Experimentation

Throughout the discussion of experimental results in this thesis, several suggestions were made as to how to improve or further research into flexible syntactic foams and their implementation into diving wetsuits, including:

- Improvements to modeling flexible geometries
- Improvements to fabrication of HGM composite materials themselves
- Improvements to wetsuit prototyping and standardization
- Further microscopy
- Further thermal and mechanical characterization
- Further field testing

5.1.1 Improvements to Modeling of Flexible Geometry

A broader ergonomic study is needed to determine a more accurate distribution of human body curvatures. The distribution in this thesis only informs the model's design for one body. Sampling from more subjects or a literature review of previous ergonomic studies for diving wetsuits is needed for more accurate designs that converge to most body types.

Besides radii of curvature, the shape of the teeth and their grooves can be modified to create better thermal contact between teeth, in order to reduce the influence of air pockets between grooves on insulance results and field tests. The redesign of the tooth structures may also reduce the stress concentrations at the tooth grooves as well. Modeling these stress concentrations and the localized stresses of HGM, similar to methods done in [23], may also be done to quickly measure the effects of structural parameters without building new molds.

5.1.2 Improvements to Fabrication of HGM composite materials

While creating bulk sample molds allowed multiple composite pieces to be produced from one, the size of these molds was limited by the volume of material that could be reasonably produced before the material became unpourable. The space in the desiccator and oven were also limited. The ability to apply a vacuum to the material as it cures, through e.g. vacuum bag sealing, may further reduce sample porosity and the variability of the flexible composite's Θ with depth.

5.1.3 Improvements to Wetsuit Prototyping and Standardization

The expectation with custom fabrication is that the fit is tailored to an individual. While the diving community in Monterey, CA has many resources available to customize wetsuits, a single wetsuit tailor may not have the capability to keep up with prototyping. Some features on the BARE 8/7, such as the integrated hood and embedded minerals within the neoprene may also make comparisons unfair. The embedded minerals claim to reflect radiated heat back to the diver, but radiative heat losses were considered to be negligible during the experiment. Partnering with a specific wetsuit company to build on their three millimeter wetsuits and then comparing those composite suits to the same company's thicker wetsuits may improve consistency among prototypes.

Also, as research students come and go from NPS, they often cannot continue valuable research in new prototype iterations. Having a standard set of diving subjects may make field results easier to compare. To improve the impact of the project, a professional diving unit can partner with this NPS project. The suits can be designed and field tested with these experts rather than students. Divers from the Navy's Experimental Diving Unit may provide greater insights from their personal experience. With their expertise, they also may be able to diagnose issues with the prototype better than graduate students.

5.1.4 Further Microscopy

While the new degassing method reduced the size of pores among composite samples, optical microscope images were insufficient in determining the loading of the HGM the size of new pores. Low magnification images on a Scanning Electron Microscope (SEM) may provide clearer, more zoomed in pictures of the new pores as well as their loading.

5.1.5 Further Thermal and Mechanical Characterization

More Θ data can be collected at pressures greater than 276 kPa (40 psi) by replacing the pressure vessel's worn gasket. Additionally, the impact of opening teeth and overcompressing teeth on Θ can be measured by placing flexible samples in jigs, designed with radii of curvature more or less than their own.

5.1.6 Further field testing

Due to time constraints, further field tests with the composite suit prototype in this thesis were not completed. Ultimately, the suit needs to be fixed at the seals (especially the neck seal) before more tests can be safely done. Based on the damage experienced by the suit from repeated wear, the entire suit may need to be deconstructed. Based on a failure analysis, the teeth can be redesigned.

5.2 New Fields of Research

This thesis also has also provided a systematic method to produce and test composite wetsuit materials, specific to diver occupation.

5.2.1 Flexible Heterogeneous Composites

Depending on the desired diving application, a heterogeneous composite containing more additives in addition to the HGM can be cast in the new composite architecture. Modifying the percentage of each of the additives can be correlated with design criteria valued by different diving communities.

5.2.2 Sonic and Ballistic Protection

For example, SEAL and Explosive Ordnance Disposal (EOD) divers may desire a suit that includes hard ceramic beads for sonic and ballistic protection. Combat divers may come under fire while swimming in the water. Larger caliber bullets from sniper rifles or large machine guns often shatter on impact, but their shrapnel can injure or kill divers. In contrast, smaller ammunition from pistols or sub-machine-guns stay intact and can penetrate the water to directly hit a diver. The current composite pieces cover vital organs across the

chest, gut, and back. Adding ballistic protection in addition to thermal protection in these areas may save a diver's life in a combat situation.

With this idea in mind, the flexible composite concept can be utilized to combine ceramics, used for ballistic protection, with ceramics, used for thermal insulation. Large beads can dropped into the tooth cavities, after the HGM composite is poured. When the solid ceramic beads occupy space at the bottom of the tooth, the glass composite will rise. As a result, less HGM composite material may need to be mixed and desiccated (a time consuming process). Conversely, finer solid, hard ceramic powders can be uniformly mixed with the HGM in the planetary centrifuge. This complete mixture can be desiccated as one mixture, as outlined in this thesis. Another idea could be to desiccate two separate mixtures of hollow glass in a carrier polymer and solid ceramic in a carrier polymer. After degassing both separately, the two mixtures are layered like a laminate. This method may reintroduce air into the composite, leading to greater porosity. Another method for degassing the mixture, possibly while being cured may be investigated to mitigate this issue. Controlling the layer thickness may also need to be investigated to successfully create laminate heterogeneous composites. A schematic of these heterogeneous composite concepts is included in Figure 5.1

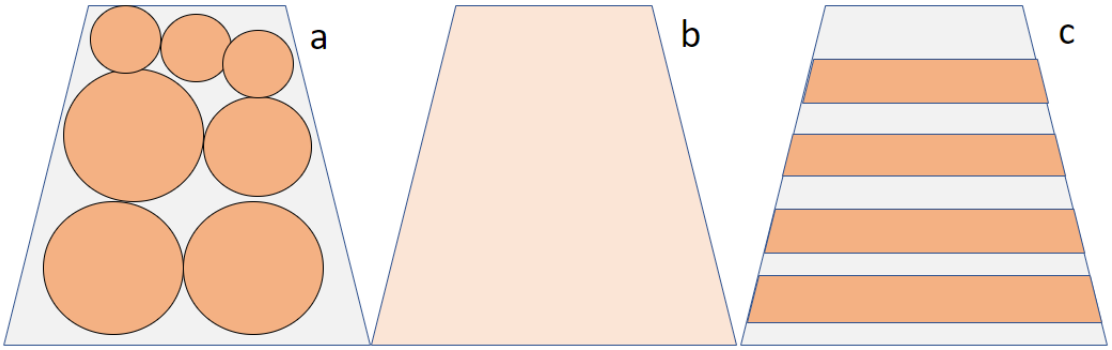

Figure 5.1. (a) Hollow Glass Microsphere and Solid Hard Ceramic Tooth (b) Uniform Mixture of Glass and Hard Ceramic (c) Laminate of Glass and Hard Ceramic

Samples with varying weight percentages of solid ceramic beads and HGM can also be cast in pucks, similar to experiments in [21], to determine how the ratio of HGM to solid

ceramics affects Θ with increasing depth. This experiment can then be related to a ballistics test of the effect of small arms ammunition on similar puck samples. Once the appropriate ratio between the two ceramics is determined, this material can be applied to chocolate bar geometry.

Adding heavier, solid ceramic beads to the composite may also counter the buoyancy that the current homogeneous HGM composite pieces add to the wetsuit.

5.2.3 Flexible Biomimetic Composites

Through biomimetics natural phenomenon are mimicked and applied to technology. In this project, more complex tooth array geometries, inspired by seal skin [29], may be explored to develop more flexible composites with better thermal insulation. Aquatic mammals rely on a layer of blubber, a layer of fur, or a combination of the two to insulate their bodies. Blubber provides a large thermal gradient between the animal's core body temperature and the surrounding ambient water temperature. However, blubber requires a much greater thickness than fur to gain these thermal benefits. Fur is much lighter and performs better in air, but in water fur compresses unlike blubber [30]. A schematic of this biological process, specifically for harbor seals, is included in Figure 5.2.

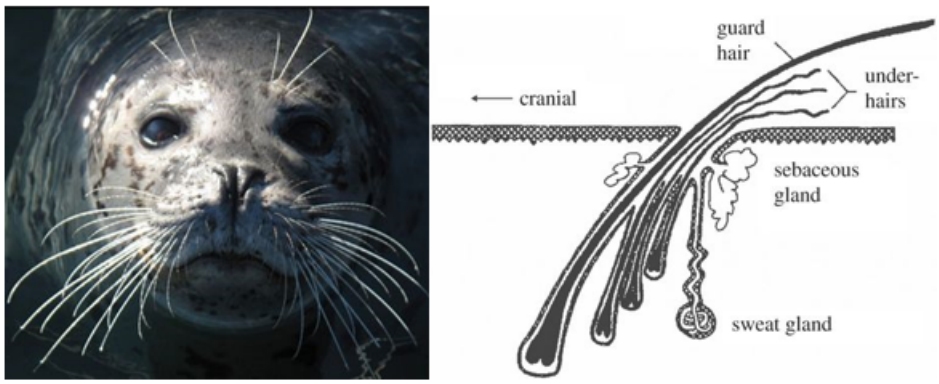

Figure 5.2. Seal Skin Schematic. Source: [29]

Both blubber and fur are used as insulation. Skin lobes or vibrissal pads on the seal's skin contain dense hair clumps. These skin lobes and the hair bundles on them direct water flow

to reduce drag. This mechanism also lessens convective heat losses across the seal's skin. Additionally the underhairs beneath the guard hair entrap water, which is heated next to the body, similar to a wetsuit. Different sized skin lobes were observed on the seal's skin. Mammals like harbor seals rely on their blubber and fur as thermal protection in cold water. Like neoprene a harbor seal's fur also compresses with depth and loses some of its thermal protection. Applying seal skin morphology to diving wetsuits for combat swimmers like SEALs would be fitting.

5.2.4 Embedded Sensor Composites

Electronics can also be embedded within the tooth array as a feature to track diver performance. Dive supervisors may be able to track these metrics, measured within diving suits, to better protect divers on jobs.

CHAPTER 6:
Conclusion

Building on previous NPS wetsuit prototypes and research into the insulative properties of HGM syntactic foams with depth, a method to universally cast stiff composites of patterned geometries that adapt to body curves was developed. In the patterned geometry, an array of trapezoidal teeth on a thin base converged or opened to approximate a body curve. Previous composite wetsuits individually cast HGM composites to exact diver shapes, rendered from 3D body scans. To achieve broader coverage schemes on a composite wetsuit with an individual casting method requires many large, expensive molds for a single diver, while the new flexible composite concept only requires two variations that can be used for many divers. Two molds were 3D printed in solid polycarbonate for cylindrical body approximations, with a minimum radius of curvature of 50 mm, and for broad body curves, with a minimum radius of curvature of 250 mm. Samples of the new composite architecture were characterized thermally and mechanically. Large bulk samples of material were cast and cut into multiple pieces to fabricate a composite wetsuit prototype. This prototype was then field tested in a real ocean environment and compared to a BARE 8/7 mm wetsuit.

The resulting universal composite samples performed as intended, converging to a wide range of body curvatures. Thermal characterization of the composite in curved orientations showed comparable insulance measurements to flat puck samples with an ideal loading of 43% vol. HGMs. The air gaps between the trapezoidal teeth negatively influenced the composite's depth independence, but to a lesser degree than neoprene for low porosity samples. With a mean thermal insulance of 0.04 $\frac{Km^2}{W}$ at 20.54 msw, high porosity samples had similar properties to neoprene. In contrast, low porosity samples had a mean insulance of 0.08 $\frac{Km^2}{W}$ at the same pressure, similar to solid puck samples.

Pores observed visually and through optical microscopy were also mechanically unfavorable. Large millimeter sized pores created large surface defects, where stresses could concentrate. Thinner grooves became more susceptible as less stress was required to yield thin wall syntactic foams. The groove geometry was also a source of stress concentrations. Results from uniaxial compression tests show that pore reduction led to higher stiffness and

densification strain. High porosity samples had much smaller elastic regions and yielded sooner than low porosity samples.

Field tests of a BARE 8/7 mm neoprene wetsuit and a flexible composites demonstrate the thermal performance of both diving suits in real seawater environments. Suits were tested separately by the same diver. ΔT measurements between the inside and outside temperatures of both suits was higher initially than previous prototype field testing. The neoprene suit had a consistent ΔT curve across three dives that steadies to approximately 20 °C. Due to a compromised neck seal, stemming from a poorly fitting diving hood, the ΔT measurements for the composite suit show rapid cooling of the body underwater and gradual rewarming at the surface, likely due to shivering. Despite the suit's loss of integrity, the minimum ΔT for the composite suit was approximately 8 °C, which is only 2 °C less than previous field testing data. Further testing with a full composite suit highlighted the need for more field testing. The results of this experiment showed large degradation of the suit, possibly due to the mechanical failure of the grooves from previous dives, resulting in a ΔT of 3 Deg C. More testing, material characterization, and standardization is needed to accurately compare HGM composite suits to conventional neoprene suits. Despite this overwhelming need for more data, the flexible composite geometry opens many research opportunities to experiment with other materials and to create diving wetsuits with properties specific to naval occupations.

APPENDIX A:
MATLAB Code for Body Parameters

```
% Andrew Waldron
% Flexible Composite Wetsuit
clear
close all
clc

% Load Body Measurement Data
data=(xlsread('Body Measurements II'));
% Define Data Features
thick= 3;  %[mm] Wetsuit Thickness
%Circumference of Cylindrical Features [mm]
circ_cyl=data(1:105, 1)./0.0393701;
circ_fore=data(1:26,1)./0.0393701;
circ_thigh=data(27:69,1)./0.0393701;
circ_shins=data(70:91,1)./0.0393701;
circ_bicep=data(92:105,1)./0.0393701;

arc_chest= data(107:138, 1)./0.0393701;
chord_chest= data(107:138, 2)./0.0393701;

% Radius of Curvature for Cylindrical Features
radii_cyl=circ_cyl/(2*pi);
%[mm] Radius of Curvature all Cylindrical Features
radii_fore= circ_fore/(2*pi)+thick;
%[mm] Radius of Curvature of Forearms
radii_thigh= circ_fore/(2*pi)+thick;
%[mm] Radius of Curvature of Thighs
radii_shins= circ_fore/(2*pi)+thick;
%[mm] Radius of Curvature of Shins/Calves
radii_bicep= circ_fore/(2*pi);
%[mm] Radius of Curvature of Bicep.
%Bicep Measurements taken with suit on.

```

```
radii_chest=ones(1,length(arc_chest));
chord_calc=2*radii_chest.*sin(arc_chest./(2*radii_chest));
tol=1e-4; % Tolerance
inc=1e-5; % Incremental Change in Radius of Curvature [mm]

for n=1:length(chord_chest)
    if arc_chest(n)<= chord_chest(n)
    %Physically if arc=chord then radius is infinite
        radii_chest(n)= NaN;
    else
       while abs(chord_calc(n)-chord_chest(n))>=tol
          radii_chest(n)= inc+ radii_chest(n);
          chord_calc(n)= 2*radii_chest(n)...
          .*sin(arc_chest(n)./(2*radii_chest(n)));
       end
    end
end
radii_chest=rmmissing(radii_chest); %Eliminates NaN from set

%% Analysis
clf
figure(1)
hold on
hist_cyl=histogram(radii_cyl);
hist_cyl.BinWidth=50;

% hist_fore=histogram(radii_fore);
% hist_fore.BinWidth=0.5;
%
% hist_thigh=histogram(radii_thigh);
% hist_thigh.BinWidth=0.5;
%
% hist_shins=histogram(radii_shins);
% hist_shins.BinWidth=0.5;
%
% hist_bicep=histogram(radii_bicep);
% hist_bicep.BinWidth=0.5;

hist_chest=histogram(radii_chest);
hist_chest.BinWidth=50;
```

```
74 title('Histogram: Body Measurements')
75 xlabel('Radius of Curvature (mm)')
76 ylabel('Number of Occurences')
77 legend('Cylindrical', 'Chest/Back/Abs')
78 % legend('Forearm', 'Thighs', 'Shins', 'Biceps', 'Chest/Back')
79
80 mu_cyl=mean(radii_cyl);     %[in] Mean of the Cylindrical Radii
81 mu_chest=mean(radii_chest); %[in] Mean of the Chest/Back Radii
82 sigma_cyl=std(radii_cyl);
83 sigma_chest=std(radii_chest);
84
85 % Ashman's D shows separation between datasets if D>2
86 D=sqrt(2)*abs(mu_cyl-mu_chest)/sqrt(sigma_cyl^2+sigma_chest^2);
87
88 figure(2)
89 hold on
90 % Scatter Plot
91 plot(radii_cyl,'x')
92 plot(radii_chest,'o')
93 % Plot Mean Lines
94 plot([0, length(radii_cyl)],[mu_cyl, mu_cyl],'k')
95 plot([0, length(radii_chest)],[mu_chest, mu_chest],'k')
96
97 % Plot Two Standard Deviations for Outlier Analysis
98 plot([0, length(radii_cyl)],...
99 [mu_cyl+2*sigma_cyl, mu_cyl+2*sigma_cyl],'b--')
100 plot([0, length(radii_cyl)],...
101 [mu_cyl-2*sigma_cyl, mu_cyl-2*sigma_cyl],'b--')
102 plot([0, length(radii_chest)],...
103 [mu_chest+2*sigma_chest, mu_chest+2*sigma_chest],'r--')
104 plot([0, length(radii_chest)],...
105 [mu_chest-2*sigma_chest, mu_chest-2*sigma_chest],'r--')
106
107 xlabel('Sample Number')
108 ylabel('Radius of Curvature (mm)')
109 legend('Cylindrical', 'Chest/Back/Abs',...
110 '\mu_{cylindrical}', '\mu_{chest}',...
111 '+2\sigma_{cylindrical}','-2\sigma_{cyl}',...
112 '+2\sigma_{chest}','-2\sigma_{chest}',...
113     'Location','Northeast')
```

```
114 axis([0, length(radii_cyl), 0, max(radii_chest)+5])
115
116 %% Outlier Elimination
117 % Upper and Lower 99% Limits for Chest
118 lim=[mu_chest+2*sigma_chest, mu_chest-2*sigma_chest];
119 iValue= radii_chest<=lim(1) & radii_chest>=lim(2);
120 radii_chest=radii_chest(iValue);
121 mu_chest=mean(radii_chest);
122 sigma_chest=std(radii_chest);
123
124 figure(3)
125 hold on
126 % Scatter Plot
127 plot(radii_cyl, 'x')
128 plot(radii_chest,'o')
129
130 % Plot Mean Lines
131 plot([0, length(radii_cyl)],[mu_cyl, mu_cyl],'k')
132 plot([0, length(radii_chest)],[mu_chest, mu_chest],'k')
133
134 % Plot Two Standard Deviations for Outlier Analysis
135 plot([0, length(radii_cyl)],...
136 [mu_cyl+2*sigma_cyl, mu_cyl+2*sigma_cyl],'b--')
137 plot([0, length(radii_cyl)],...
138 [mu_cyl-2*sigma_cyl, mu_cyl-2*sigma_cyl],'b--')
139 plot([0, length(radii_chest)],...
140 [mu_chest+2*sigma_chest, mu_chest+2*sigma_chest],'r--')
141 plot([0, length(radii_chest)],...
142 [mu_chest-2*sigma_chest, mu_chest-2*sigma_chest],'r--')
143
144 xlabel('Sample Number')
145 ylabel('Radius of Curvature (mm)')
146 legend('Cylindrical', 'Chest/Back/Abs', '\mu_{cylindrical}',...
147 '\mu_{chest}','+2\sigma_{cylindrical}',...
148 '-2\sigma_{cyl}','+2\sigma_{chest}','-2\sigma_{chest}',...
149     'Location','Northeast')
150 axis([0, length(radii_cyl), 0, max(radii_chest)+50])
151
152
153 %% Table of Characteristics
```

```
154 table(mu_cyl, sigma_cyl, mu_cyl+2*sigma_cyl,...
155 mu_cyl-2*sigma_cyl, mu_chest, sigma_chest,...
156 mu_chest+2*sigma_chest, mu_chest-2*sigma_chest,...
157 'VariableNames', {'\mu_{cyl}','\sigma_{cyl}',...
158 '\mu_{cyl}+2\sigma', '\mu_{cyl}-2\sigma',...
159 '\mu_{chest}','\sigma_{chest}',...
160 '\mu_{chest}+2\sigma', '\mu_{chest}-2\sigma'})
```

THIS PAGE INTENTIONALLY LEFT BLANK

APPENDIX B:
Flexible Composite Piece Material Measurements

Table B.1. Wetsuit Cylindrical Composite Piece Measurements

	m_{binder} [g]	$m_{polymer}$ [g]	m_{glass} [g]
1	9.09	91.05	10.02
	9.10	91.50	10.02
	9.18	92.04	9.99
	9.30	94.72	9.99
	9.49	95.12	10.00
	9.06	90.19	9.98
2	9.09	91.02	10.00
	9.12	91.50	10.02
	9.05	91.25	9.98
	9.12	91.72	9.99
	9.09	91.26	9.99
3	9.22	92.93	10.01
	9.38	92.88	9.99
	9.07	90.75	10.01
	9.08	90.75	10.00
	9.06	91.12	10.01
4	9.02	89.72	9.99
	9.02	90.44	9.99
	9.00	92.23	10.03
	9.03	90.28	10.00
5	9.05	90.93	10.01
	9.20	93.31	10.02
	4.64	48.99	5.01
	9.01	90.98	10.04
	9.44	95.12	10.00
6	9.02	90.25	10.00
	9.10	91.24	10.01
	9.00	90.96	9.99
	9.02	90.12	10.00
7	9.03	90.92	10.02
	9.10	91.29	9.98
8	9.38	93.41	10.01
	9.03	90.79	10.01
	9.31	92.85	10.00

Table B.2. Wetsuit Broad Composite Piece Measurements

	m_{binder} [g]	$m_{polymer}$ [g]	m_{glass} [g]
9	9.15	91.87	10.02
	9.04	91.68	10.01
	9.05	91.74	9.98
	9.12	91.05	10.01
	9.23	93.35	9.99
	9.01	90.71	9.98
	9.27	91.86	10.00
	9.16	91.29	10.01
	9.26	92.60	10.00
10	9.06	90.51	10.01
	9.07	90.78	10.00
	9.25	92.87	10.00
	9.09	91.61	10.01
	9.32	93.69	10.01
	9.06	90.58	9.99
	9.23	93.83	10.02
	9.21	92.01	10.03
	9.08	91.36	10.00
11	9.06	90.72	10.01
	9.11	93.26	10.01
	9.02	91.17	10.02
	9.06	91.11	10.00
	9.05	90.92	10.00
	9.12	93.40	9.99
	9.40	95.02	10.00
	9.13	91.92	9.99
	9.28	96.60	9.98

APPENDIX C:
Machining Plans for Jigs

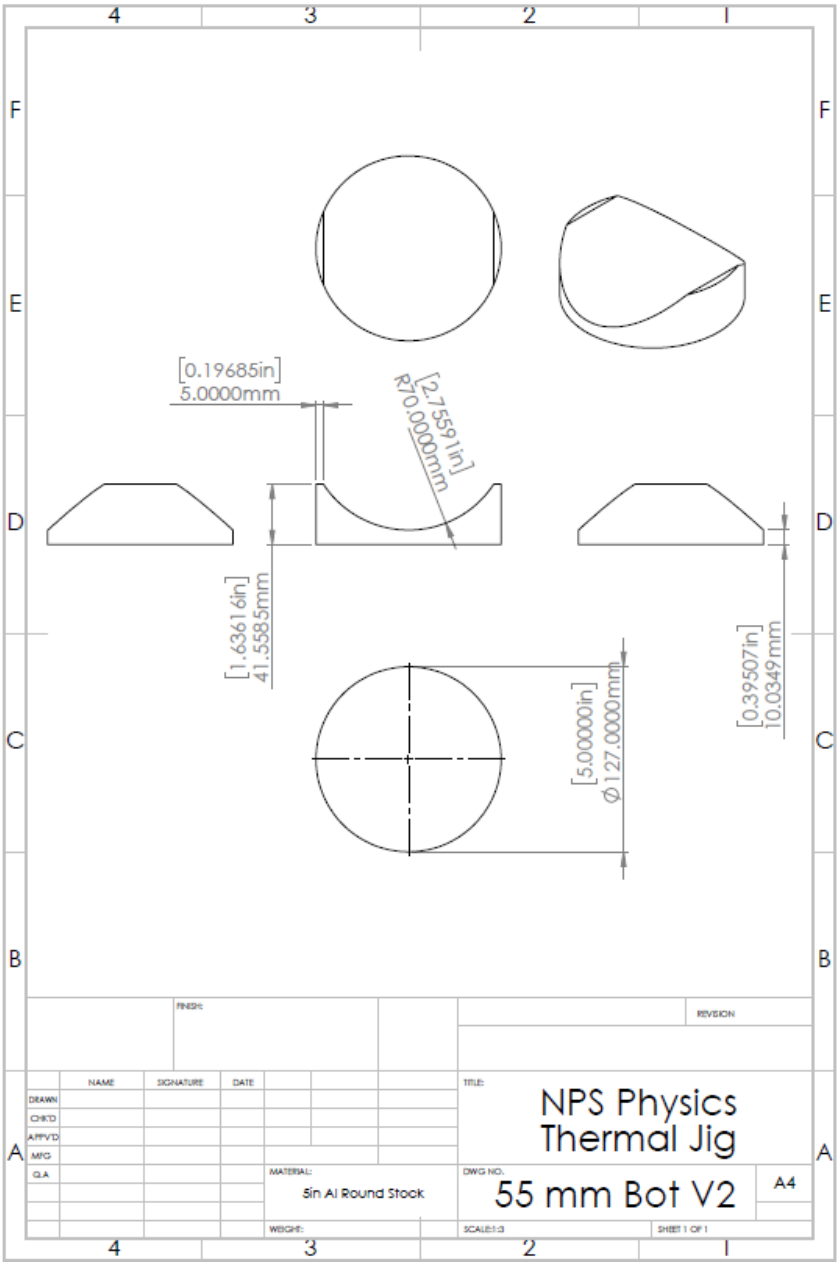

Figure C.1. Jig Bottom for Composite with r=50 mm

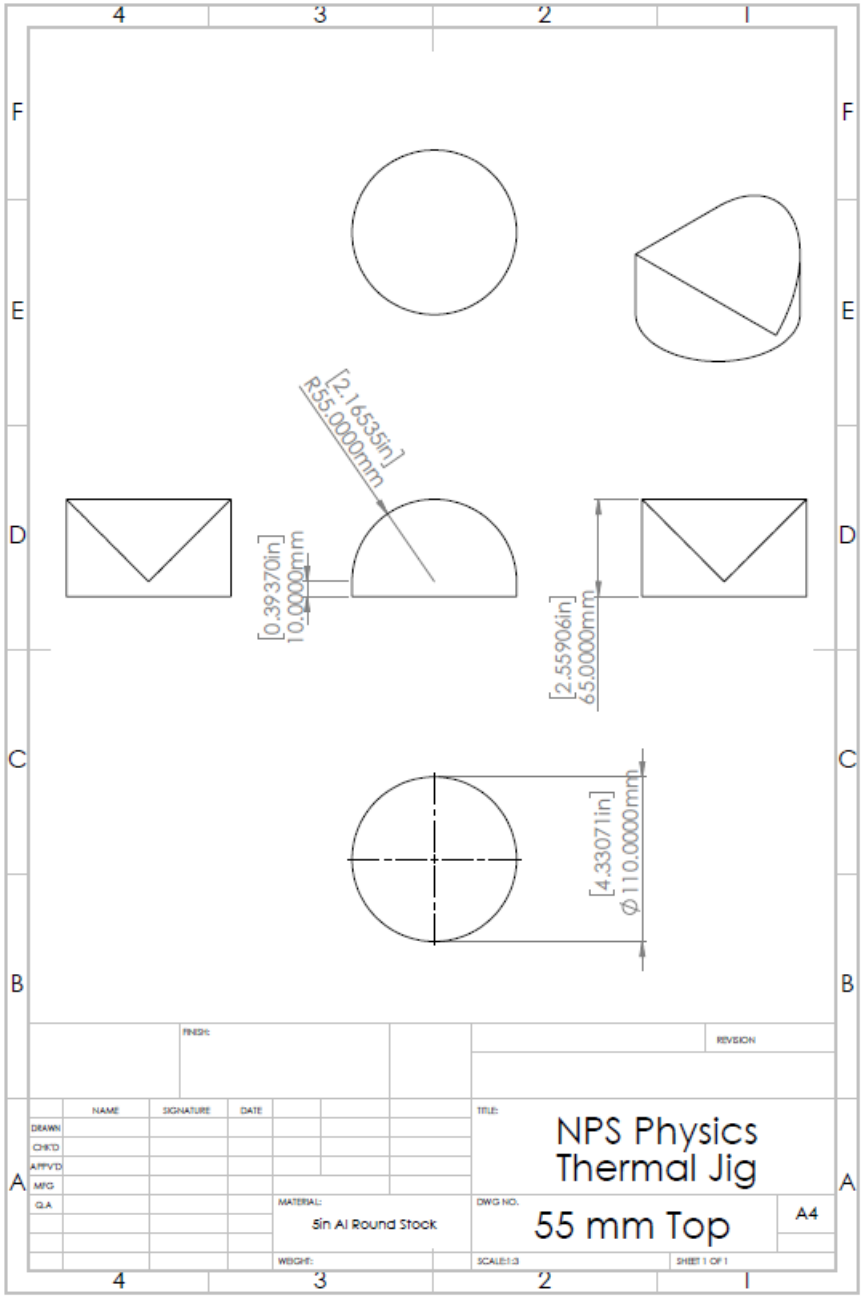

Figure C.2. Jig Top for Composite with r=50 mm

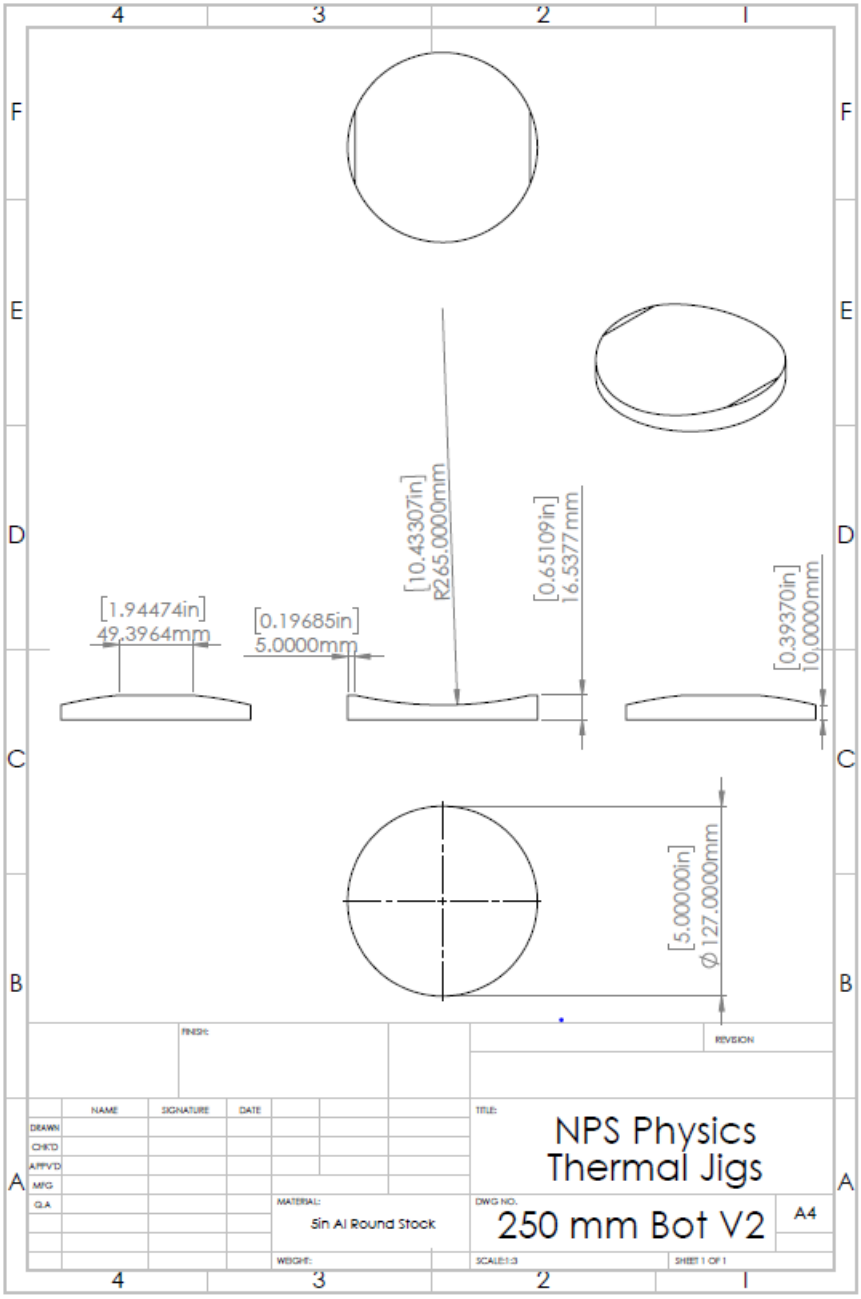

Figure C.3. Jig Bottom for Composite with r=250 mm

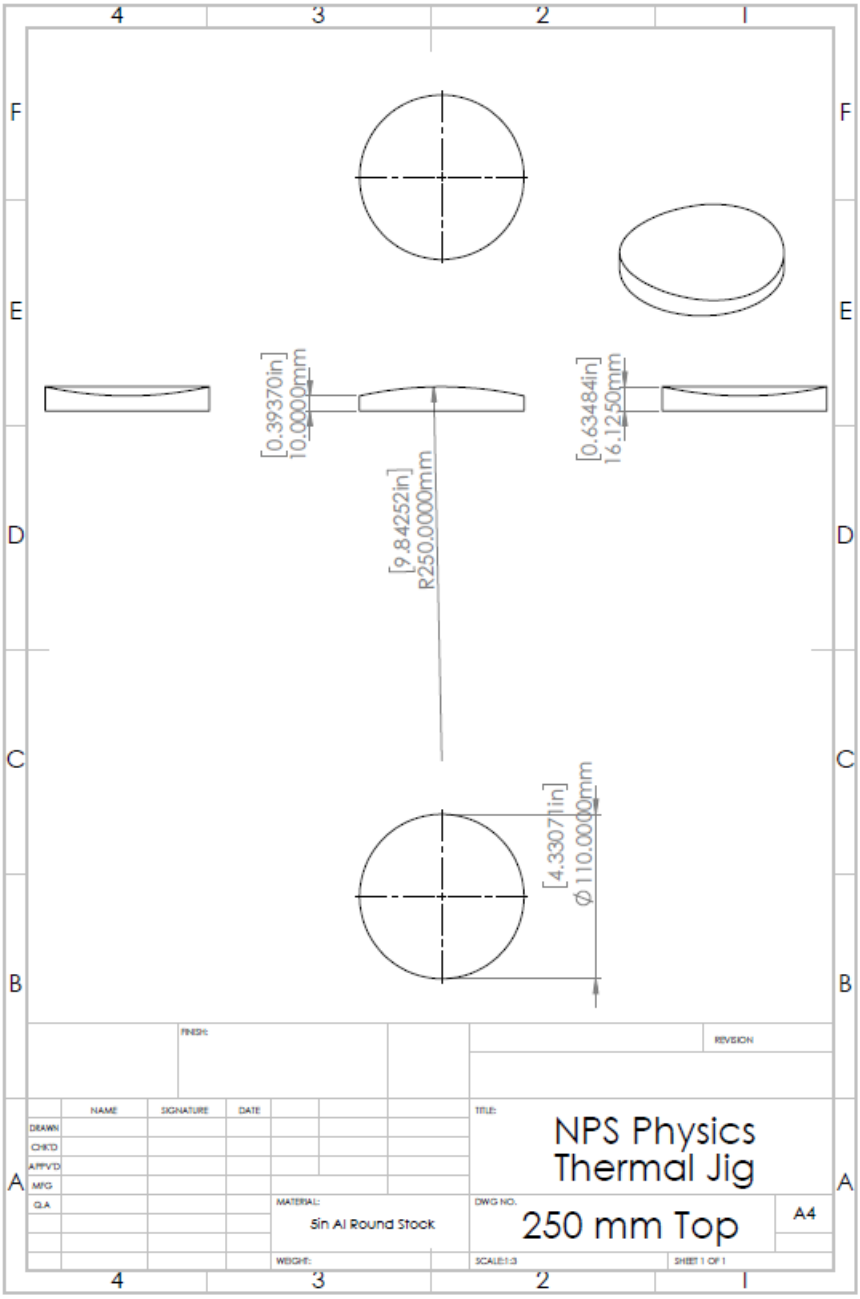

Figure C.4. Jig Top for Composite with r=250 mm

APPENDIX D:
SCUBA Field Test Safety Log

Date	Max Depth	Bottom Time	Start Bottle Pressure	End Bottle Pressure
	msw	min	bar	bar
16 APR	8	28	227.5	124.1
20 APR	12	25	227.5	151.6
20 APR	9	26	151.6	55.1
14 MAY	14	15	206.8	117.2
14 MAY	12	20	117.2	34.5
15 MAY	15	30	206.8	34.5
26 MAY	13	35	206.8	41.3

THIS PAGE INTENTIONALLY LEFT BLANK

List of References

[1] "Diving in the U.S. Navy: A Brief History," Naval History and Heritage Command, Sep. 7, 2017 [Online]. Available: https://www.history.navy.mil/research/library/online-reading-room/title-list-alphabetically/d/diving-in-the-u-s-navy-a-brief-history.html

[2] D. Larter and M. Meyers, "Navy seals set to open up to women, top admiral says," Navy Times, Aug. 18, 2015 [Online]. Available: https://www.navytimes.com/news/your-navy/2015/08/18/navy-seals-set-to-open-to-women-top-admiral-says/

[3] "This navy diver's story of disorientation 190 feet down is full of nope," Youtube, Apr. 28, 2022 [Online]. Available: https://www.youtube.com/watch?v=S2yhU1KHoHM

[4] J. Clark, "This navy diver's story of disorientation 190 feet down is full of nope," Task and Purpose, Apr. 10, 2017 [Online]. Available: https://taskandpurpose.com/community/navy-divers-disorientation-deep-sea-diving/

[5] C. Rainey, "Wet suit pursuit: Hugh bradner's development of the first wet suit," Scripps Institution of Oceanography, San Diego, CA, Tech. Rep., 1998. Available: https://escholarship.org/uc/item/7353g3dj

[6] N. Patch, "Bakuhatai:the reconnaissance mission of the uss burrfish and the fate of three american pow," National Archives, Nov. 3, 2016 [Online]. Available: https://www.archives.gov/files/publications/prologue/2015/winter/bakuhatai.pdf

[7] D. Camp and S. P. Camp, "Frogmen were the first on iwo jima," Veterans of Foreign Wars, Feb. 14, 2020 [Online]. Available: https://www.vfw.org/media-and-events/latest-releases/archives/2020/2/frogmen-were-the-first-on-iwo-jima

[8] *U.S Navy Diving Manual*, 7th ed., Naval Sea Systems Command, 2016.

[9] "The skin they're in: U.s. navy diving suits," Naval History and Heritage Command, Nov. 3, 2016 [Online]. Available: https://www.history.navy.mil/content/history/museums/undersea/explore/exhibits/online/the-skin-theyre-in/skins-navy-divers-work-in.html

[10] M. Aguilella-Arzo, A. Alcaraz, and V. Aguilella, "Heat loss and hypothermia in free diving: Estimation of survival time under water," *American Journal of Physics*, vol. 71, no. 333, Apr 2003 [Online]. doi: https://doi.org/10.1119/1.1531581.

[11] J.-P. Rodrigue, "Chapter 5 - maritime transportation," in *The Geography of Transport Systems (Fifth Edition)*. New York, NY, USA: Routledge, 2020. Available: https://transportgeography.org/contents/chapter5/maritime-transportation/draft-containership-capacity/

[12] E. Bardy, J. Mollendorf, and D. Pendergast, "Thermal conductivity and compressive strain of foam neoprene insulation under hydrostatic pressure," *Journal of Physics D: Applied Physics*, vol. 38, no. 20, Sep 2005 [Online]. doi: https://doi.org/10.1088/0022-3727/38/20/009.

[13] N. Conner, "What is r-value – thermal insulance factor – definition," Thermal Engineering, May. 22, 2019 [Online]. Available: https://www.thermal-engineering.org/what-is-r-value-thermal-insulance-factor-definition/

[14] F. L. Beckman, "Thermal protection during immersion in cold water," Navy Medical Research Institute, Bethesda, MD: USA, 1964 [Online]. Available: https://apps.dtic.mil/sti/pdfs/AD0601044.pdf

[15] R. Nostrant, "Navy divers recover torpedos under arctic ice during icex," Navy Times, Mar. 16, 2022 [Online]. Available: https://www.navytimes.com/news/your-navy/2022/03/16/navy-divers-recover-torpedoes-under-arctic-ice-during-icex/#:~:text=Navy%20divers%20took%20to%20the,participating%20in%20the%20biennial%20exercise

[16] P. Kosky, R. Balmer, W. Keat, and G. Wise, "Chapter 12 - mechanical engineering," in *Exploring Engineering (Third Edition)*, P. Kosky, R. Balmer, W. Keat, and G. Wise, Eds. Boston, MA, USA: Academic Press, 2013, pp. 259–281.

[17] T. Bergman, A. Lavine, F. Incropera, and D. Dewitt, "Chapter 3 - one-dimensional, steady-state conduction," in *Introduction to Heat Transfer (Sixth Edition)*, L. Ratts and R. Marchione, Eds. Hoboken, NJ, USA: Wiley, 2011, pp. 112–192.

[18] A. Kwong-Wright, "Composite thermal wetsuit," M.S. thesis, Dept. of Physics, NPS, Monterey, CA, USA, 2021.

[19] S. Martin, "Building and testing an incompressible thermally insulating cold temperature diving wetsuit," M.S. thesis, Dept. of Physics, NPS, Monterey, CA, USA, 2020.

[20] "Monterey," Sea Temperature, 2022 [Online]. Available: https://seatemperature.net/current/united-states/monterey-california-united-states-sea-temperature#:~:text=Average%20annual%20water%20temperature%20on,60%C2%B0F)%20in%20August.

[21] J. Brown, J. Oldenkamp, R. Gamache, D. Grbovic, and E. Kartalov, "Hollow-microsphere composite offers depth-independent superior thermal insulation for diver suits," *Materials Research Express*, vol. 6, no. 5, Feb 2019 [Online]. doi: https://doi.org/10.1088/2053-1591/ab0447.

[22] E. Bardy, J. Mollendorf, and D. Pendergast, "A comparison of the thermal resistance of a foam neoprene wetsuit to a wetsuit fabricated from aerogel-syntactic foam hybrid insulation," *Journal of Physics D: Applied Physics*, vol. 39, no. 18, Sep 2006 [Online]. doi: https://doi.org/10.1088/0022-3727/39/18/018.

[23] S. S. M. D. Pavana Prabhakar, Haotian Feng, "Densification mechanics of polymeric syntactic foams," *Composites Part B: Engineering*, vol. 232, Mar 2022 [Online]. doi: https://doi.org/10.1016/j.compositesb.2021.109597.

[24] M. E. Hoque, W. San, F. Wei, S.-M. Li, M.-H. Huang, M. Vert, and D. Hutmacher, "Processing of polycaprolactone and polycaprolactone-based copolymers into 3d scaffolds, and their cellular responses," *Tissue engineering. Part A*, vol. 15, Apr 2022 [Online]. doi: https://doi.org/10.1089/ten.TEA.2008.0355.

[25] "6 cell medium chocolate bar candy mold professional silicone artisan mould cake," Joom, Oct. 4, 2021 [Online]. Available: https://www.joom.com/en/products/5c1b6af236b54d0101474a77

[26] "Fortus 450mc," Stratsys, 2022 [Online]. Available: https://www.stratasys.com/en/3d-printers/printer-catalog/fdm-printers/fortus-450mc/

[27] "3m™ glass bubbles k1," 3M, 2022 [Online]. Available: https://www.3m.com/3M/en_US/p/d/b40064615/

[28] "Stay warm in the water ultrawarmth ensures warmer, longer dives," BARE, 2022 [Online]. Available: https://www.baresports.com/ultrawarmth-technology/?v=7516fd43adaa

[29] N. Erdsack, G. Dehnhardt, M. Witt, A. Wree, U. Siebert, and W. Hanke, "Unique fur and skin structure in harbour seals (phoca vitulina)—thermal insulation, drag reduction, or both?" *Journal of The Royal Society Interface*, vol. 12, no. 104, Mar 2015 [Online]. doi: https://doi.org/10.1098/rsif.2014.1206.

[30] H. E. M. Liwanag, A. Berta, D. P. Costa, S. M. Budge, and T. M. Williams, "Morphological and thermal properties of mammalian insulation: the evolutionary transition to blubber in pinnipeds," *Biological Journal of the Linnean Society*, vol. 107, no. 4, Dec 2012 [Online]. doi: https://doi.org/10.1111/j.1095-8312.2012.01992.x.

THIS PAGE INTENTIONALLY LEFT BLANK

Initial Distribution List

1. Defense Technical Information Center
   Ft. Belvoir, Virginia

2. Dudley Knox Library
   Naval Postgraduate School
   Monterey, California